Water Resources Research

RESEARCH ARTICLE
10.1029/2020WR028394

Impact of Vegetation Physiology and Phenology on Watershed Hydrology in a Semiarid Watershed in the Pacific Northwest in a Changing Climate

Bowen Zhu[1,2], Maoyi Huang[1,3], Yanyan Cheng[1], Xianhong Xie[2], Ying Liu[1], Gautam Bisht[1], and Xingyuan Chen[1]

[1]Atmospheric Sciences and Global Change Division, Pacific Northwest National Laboratory, Richland, WA, USA, [2]State Key Laboratory of Remote Sensing Science, Jointly Sponsored by Beijing Normal University and Institute of Remote Sensing and Digital Earth of Chinese Academy of Sciences, Beijing, China, [3]Now at Office of Science and Technology Integration, National Weather Service, National Oceanic and Atmospheric Administration, Silver Spring, MD, USA

Key Points:

- Carbon dioxide fertilization leads to increase in gross primary production and more carbon allocation to leaf biomass, therefore increased nitrogen demand uptake
- Enhanced photosynthesis leads to increased leaf area index
- The hydrologic budget over a semiarid watershed can be strongly modulated by changes in stomatal resistance and leaf area index through evapotranspiration

Supporting Information:

- Supporting Information S1
- Table S1

Correspondence to:

B. Zhu,
bwzhu@mail.bnu.edu.cn

Citation:

Zhu, B., Huang, M., Cheng, Y., Xie, X., Liu, Y., Bisht, G., & Chen, X. (2021). Impact of vegetation physiology and phenology on watershed hydrology in a semiarid watershed in the Pacific Northwest in a changing climate. *Water Resources Research*, *57*, e2020WR028394. https://doi.org/10.1029/2020WR028394

Received 20 JUL 2020
Accepted 26 JAN 2021

Abstract Changes in carbon dioxide (CO_2) concentration and nitrogen (N) availability can affect land surface processes by regulating physiological (e.g., stomatal opening and closure) and phenological (e.g., leaf area index) responses, which in turn influence terrestrial water cycle dynamics. In this study, we apply the Community Land Model version 5 to investigate how projected environment changes in the 21st century can affect the hydrologic budget in the Upper Columbia-Priest Rapids watershed, a typical semiarid watershed located in the Pacific Northwest of the United States. Nine numerical experiments were performed to quantifying contributions of climate change, CO_2 concentration, and N availability to the watershed hydrologic budget under two Representative Concentration Pathways (RCPs) (i.e., RCP4.5 and RCP8.5). Our results show that compared to its historical value, evapotranspiration (ET) over the watershed increases by 15% and 12% by the end of the century under RCP4.5 and RCP8.5 in responses to changes in meteorological forcing, and further increases by 16% and 11% when elevated CO_2 concentrations are accounted for. The effect of N availability on the water balance is insignificant. Such an increase in ET is contributed by the overall increase in leaf area index of vegetation in response to increases in precipitation and CO_2 concentration. However, corn-dominated regions can respond to these changes differently, caused by its increased stomatal resistance under an elevated CO_2 concentration with limited N. Our results demonstrate physiological and phenological responses can modulate watershed hydrologic budgets under projected future changes.

Plain Language Summary Increases in atmospheric carbon dioxide (CO_2) may affect land surface processes through changes in photosynthesis and stomatal resistance of plants. The atmospheric nitrogen (N) deposition and fertilization are major source of soil mineral N that can be directly assimilated by plants. In this study, we use the Community Land Model version 5 to investigate how climate change, atmospheric CO_2 concentration, N deposition, and fertilization rates affect hydrologic dynamics in the Upper Columbia-Priest Rapids watershed, a typical semiarid watershed located in the north-western United States. Our results show that compared to its historical value, evapotranspiration over the watershed is increased by the end of the century in responses to changes in precipitation and temperature, and elevated CO_2 concentrations. The effect of N availability on the water balance is insignificant. Such an increase in evapotranspiration is contributed by the overall increase in leaf area index of vegetation in response to increases in precipitation and CO_2 concentration. However, corn-dominated regions can respond to these changes differently, caused by its increased stomatal resistance under an elevated CO_2 concentration with limited N. Our results demonstrate physiological and phenological responses can modulate watershed hydrologic budgets under projected future changes.

1. Introduction

Climate is now changing at a faster pace than that at any point in the history. The global mean surface temperature (T) in 2006–2015 increased 0.87°C relative to the 1850–1900 condition (Hoegh-Guldberg et al., 2018). Atmospheric concentrations of greenhouse gases (GHGs) including carbon dioxide (CO_2),

nitrous oxide (N_2O), and water vapor have been increasing, and remain as the main forcing of global warming. Due to human activities (e.g., industrialization, deforestation), atmospheric CO_2 concentration has increased from 278 ppm in 1750 to 407.8 ppm in 2018, and N_2O concentration has increased to 331.1 parts per billion, which is 123% of preindustrial levels (WMO Greenhouse Gas Bulletin). The global water vapor, the largest contributor to the GHGs has also increased significantly (Chen & Liu, 2016). Such changes will continue over this century and beyond. Associated with the long-term, global scale changes, semiarid regions are projected to expand (Huang et al., 2012; Huang, Ji, et al., 2015) with exacerbated risks of land degradation and desertification in the near future (Huang, Yu, et al., 2015). Thus, the hydrological cycle could be fundamentally perturbed considering the already existing water stress in semiarid and arid regions (Abdulla et al., 2008). One example of such regions lies in the inland region of the Pacific Northwest (PNW) as part of the Columbia River Basin (CRB).

The CRB is the dominant water resources system of the PNW. River flow in the basin shows significant seasonal sensitivities to climate variability while the water management infrastructure (e.g., reservoirs and irrigation canals) buffers such sensitivities (Miles et al., 2000; Zhou et al., 2018). Reduction in water availability induced by declines in snowpack and streamflow in combination with increases in water demands observed in recent decades lead to water shortage (Dalton & Mote, 2013) that directly affects agricultural and other human activities, with important economic consequences (Rind et al., 1992). About 24% of land area in the PNW is devoted to agricultural production. While increasing atmospheric CO_2 concentration may be beneficial to crops, reduced water availability for irrigation and higher T may reduce the proportion of irrigable cropland and the value of agricultural production (Dalton & Mote, 2013; Melillo et al., 2014). Climate in the PNW is projected to experience greater warming year-round and a decrease in P in the growing season (Mote et al., 2003) that will pose huge challenges for local crop production and irrigation water supply during growing seasons. Therefore, quantifying hydrologic dynamics and their interactions with the biogeochemical cycle in a changing climate in semiarid watersheds is important for water resource and agricultural planning and management.

Numerous assessments of hydrologic and biogeochemical responses to changes in climate and GHGs emissions have been conducted in the past decade (Butcher et al., 2014; Leakey et al., 2009; Lee et al., 2010; Liu et al., 2016; Schimel et al., 2015). The warmer T and intensive P tend to lead to higher ET and runoff. For example, the global annual lake evaporation can increase by 16% by the end of the century due to warm surface T and enhanced long-wave radiation (Wang et al., 2018). However, changes in the terrestrial water cycle are not determined by climate alone and can be closely coupled to ecosystem dynamics and sequential changes in the biogeochemical cycle. For example, elevated CO_2 concentration can enhance photosynthetic capability and biomass production. Simultaneous increases in atmospheric N deposition (McCarthy et al., 2010) sustain soil mineral N that can be directly assimilated by plants. These changes in climate and environmental conditions could also boost an expansion in the leaf area, which supports more transpiration (Saxe et al., 1998). On the other hand, the increasing CO_2 concentration could induce a reduction in ET and an increase in runoff by reducing stomatal conductance (Hungate et al., 2002; Swann et al., 2016; Taub, 2010; Xu et al., 2016). Therefore, changes in terrestrial hydrologic processes and their interactions with climate, CO_2, and N limitation are complex.

Previous modeling studies on climate and GHGs effects on the hydrologic cycle are limited in terms of resolving dynamic CO_2 concentration and N availability and representing multiple croplands and land management practices. For example, Singh et al. (2020) used the CLM5 to analyze the effects of elevated CO_2 concentration on plant growth as well as the changes in streamflow in the southeastern United States. However, their study did not account for the variety of crop types and the atmospheric N deposition which could significantly decreased the degree of N limitation for plant growth (Magnani et al., 2007). Niu et al. (2013) applied the Variable Infiltration Capacity model to study the impacts of increased CO_2 concentration on hydrologic responses, but was not able to differentiate physiologic responses (e.g., changes in photosynthetic capacity and stomatal resistance) and therefore sensitivities of various crop types (Dawson et al., 2014). Crop management practices such as irrigation and fertilization that can alleviate water and nutrient stress for plants are also ignored in the model. Therefore, it remains unclear how changes in CO_2 concentration and N availability in the future can affect agro-ecosystems that strongly modulate hydrologic processes at the watershed scale.

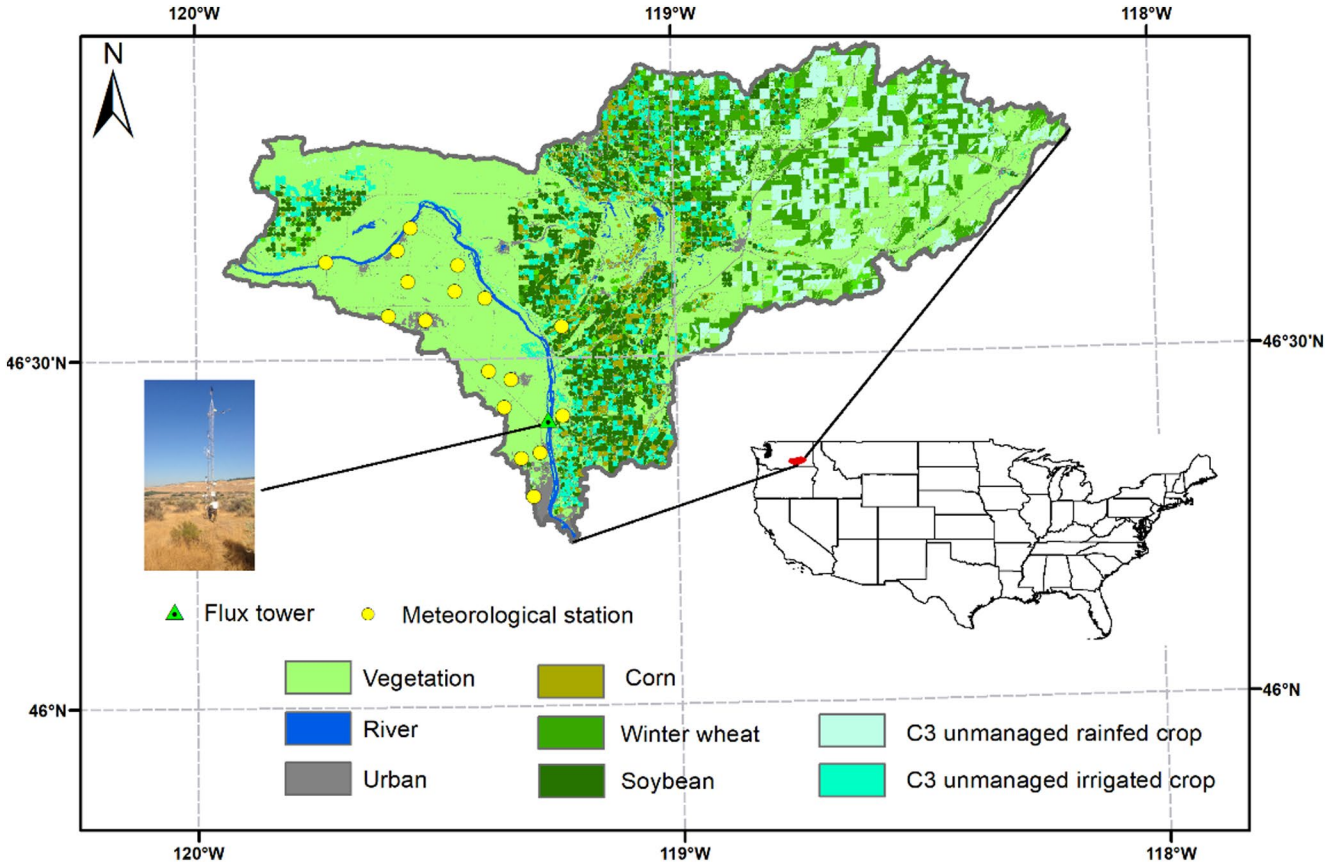

Figure 1. The location and land covers in the year 2014 of the UCPR watershed. UCPR, Upper Columbia-Priest Rapids.

In this study, we hypothesize that despite spatiotemporal variabilities over different landscapes in a semiarid watershed, cropland is the most sensitive land use type to changes in climate and associated changes in atmospheric composition (Li et al., 2011; Lovelli et al., 2010), therefore dominate watershed-scale hydrologic responses through their modulation on vegetation phenology (e.g., LAI) and physiology (e.g., stomatal resistance) on evapotranspiration. In order to quantify how hydrologic processes will change in response to climate, CO_2 concentration, and N availability over different land cover types in semiarid regions, we apply the CLM5 (Lawrence et al., 2019) in a typical semiarid agricultural watershed, the Upper Columbia-Priest Rapids (UCPR) watershed (Figure 1), a subbasin of the Columbia River basin located in the PNW of the United States. We extend a 1-km CLM5 configuration validated over the historical period (B. Zhu et al., 2020) to the end of the 21st century under different scenarios of climate, CO_2 concentration, atmospheric N deposition, and fertilization rates data sets to test our hypothesis.

In a previous study, we have applied CLM5 to simulate effects of irrigation on water, carbon, and nitrogen budgets over the period of 2010–2018. The model was configured to explicitly represent landscape heterogeneity spanning natural vegetation, corn, soybean, and urban areas, and incorporated realistic crop management practices including planting, harvesting, irrigation, and fertilization. The model is fully calibrated and validated by comparing with in situ and remotely sensed datasets. Interested readers are referred to Zhu et al. (2020) for details on model configuration and calibration.

This study is structured as follows: in Section 2, we describe numerical experiments and their driving data sets; in Section 3, the hydrological and biogeochemistry responses to climate and environmental factors over the study domain are presented. Summary on our findings and future directions will be provided in Section 4.

2. Methodology

2.1. Study Domain

The UCPR watershed is located in the southeastern of the State of Washington, a level 8 watershed according to the US Geological Survey hydrologic unit code system (https://water.usgs.gov/GIS/huc_name.html#Region17). The annual mean precipitation is less than 180 mm with most snow and rain falls in the winters or early springs (Gee et al., 2007). Cold, wet winters and hot, dry summers characterize a typical cool-desert-type climate of the region. The Columbia River flows from northwest to southwest with a length of 75 km. The eastside of the river is mainly irrigated croplands and the westside is dominated by natural vegetation, such as shrubland and grassland. Although P over the watershed is limited, benefited from irrigation water withdrawal from abundant water resources in the river and reservoirs, the study domain is one of the most productive agriculture regions in the world.

According to the USDA National Agricultural Statistics Service Cropland Data Layer (CDL) (https://nassgeodata.gmu.edu/CropScape/), a 30-m resolution land cover data set derived from satellite imagery, the UCPR watershed is covered by four major land use types, namely croplands, natural vegetation, urban, and river. Natural vegetation (e.g., shrub and grassland) and cropland account for ~90% areas in the watershed, leaving less than 10% area covered by urban and river. The area coverages of these land use types stay stable and no significant land use change has occurred in the study domain during the past decade. Corn and soybean are the major managed crops planted in the watershed, accounting for 7.8% and 21.5% over cropland areas, which require irrigation and fertilization during growing seasons. Amounts of irrigation water use for corn and soybean can reach 329 mm yr^{-1} and 394 mm yr^{-1} when averaged over the planting area of each crop, nearly double the annual mean precipitation. Winter wheat, C3 unmanaged rainfed crop (e.g., fallow/idle cropland), and C3 unmanaged irrigated crop (e.g., pasture, carrots) are located in the eastern portion of the watershed. Both winter wheat and C3 unmanaged rainfed crop only rely on snowmelt and rainfall to replete soil moisture.

2.2. Model Description

The CLM5 (Lawrence et al., 2019) model is used in this study. CLM5 is developed as the land component of the Community Earth System Model (CESM) for simulating land surface and subsurface hydrologic and biogeochemical processes, such as runoff generation, groundwater movement, surface energy fluxes, and carbon and nitrogen cycles. It has been evaluated in various studies against remote sensing datasets and flux tower measurement to analyze the sensitivity of vegetation carbon and nitrogen cycling parameters (Fisher et al., 2019), simulate effects of transient crop expansion, irrigation, and fertilizer on increasing crop yields (Lombardozzi et al., 2020), study high-latitude inundation dynamics (Ekici et al., 2019), and analyze the plant hydraulic stress effects (Kennedy et al., 2019).

CLM5 incorporates physiological and phenological representations and improved biogeochemical parameterizations of various crop types and land management practices. The time varying CO_2 concentration and deposition of reactive N are also coupled to biogeochemical cycles in CLM5. Therefore, the model is capable of jointly accounting for impacts of multiple environmental (e.g., climate, CO_2 enrichment, N availability) and anthropologic factors (e.g., irrigation and fertilization) on different crop and vegetation types, when evaluating their impacts on water, carbon, and nitrogen dynamics.

In CLM5, photosynthetic capacity and stomatal resistance can respond to changes in CO_2 concentration directly. The Leaf Utilization of Nitrogen for Assimilation module (LUNA) (Ali et al., 2016) is utilized to parameterize photosynthetic capacity of C3 natural vegetation, which is a function of CO_2 concentration, T, radiation, relative humidity, and day length (Fisher et al., 2019). The LUNA predicts an optimal partitioning of N among light capture, electron transport, carboxylation, respiration, and storage. The photosynthetic capacity of crops is estimated based on the leaf nitrogen content, the maximum rate of carboxylation, and day length. The Fixation and Uptake of Nitrogen (FUN) model is incorporated into the CLM5 to simulate plants dynamics and carbon economics of N acquisition from the environment (Fisher et al., 2019) based on work by Shi et al. (2016). In the FUN model, the amount of expenditure of energy in the form of carbon used to uptake nitrogen by plants are determined by the abundance of nitrogen in the soils and plant tissues and the

temperature-dependent cost of N fixation (Fisher et al., 2019). Plants tend to employ more carbon to acquire nitrogen where nitrogen is scarce in the environment. Furthermore, photosynthetic capability determined by these environmental factors can modulate stomatal resistance (Equation 1), because the opening and closure of stomata for photosynthesis directly change input and output rates of water vapor calculated as:

$$\frac{1}{R_s} = g_o + 1.6\left(1 + \frac{g_1}{\sqrt{D}}\right)\frac{A_n}{\frac{c_s}{P_{\text{atm}}}} \quad (1)$$

where R_s is leaf stomatal resistance (s m^2 μmol^{-1}), g_o is the i stomatal conductance (μ mol m^{-2} s^{-1}), A_n is leaf net photosynthesis (μmol CO_2 m^{-2} s^{-1}), C_s is the CO_2 partial pressure at the leaf surface (Pa), P_{atm} is the atmospheric pressure (Pa), and D is the vapor pressure deficit at the leaf surface (kPa), g_1 is a plant functional type dependent parameter.

N deposition is represented as an input to soil mineral N from the atmosphere. It is originated from the natural (e.g., lightning and wildfire) and anthropogenic (e.g., industrial processes and deforestation) sources (Galloway et al., 2004), and assumed to enter the NH_4^+ pool and vertically distributed throughout the soil profile. The sources of soil mineral N also include the mineralization from soil organic matter, biological N fixation, and fertilization. The sinks for soil mineral N are denitrification, leaching to the runoff, assimilated by plants, and wildfire (http://www.cesm.ucar.edu/models/clm/biogeochemistry.html).

2.3. Model Inputs

CLM5 require meteorological forcing and land surface characteristics as forcing or input parameters. The meteorological forcing includes P, air T, surface pressure, wind speed, relative humidity, radiation. Time series of CO_2 concentration and rate of N deposition are also applied based on scenarios chosen. The N deposition rate represents the total deposition of mineral N onto the surface and is supplied a time-varying and spatially varying for a transient simulation.

In the historical period (1985–2014), observational data from meteorological stations over the domain are used wherever available (Figure 1). We bilinearly interpolate the hourly North American Land Data Assimilation System phase 2 (NLDAS2) land-surface forcing data (1/8th degree grid) onto 1/16th degree grid over the study domain. For grid cells on the 1/16th grid which are closest to one of the 30 meteorological stations in Figure 1, we use available observations at the station to substitute the values interpolated from NLDAS2. The monthly climatology over 2000–2015 calculated based on NLDAS2 and observations from stations at the overlapping grid cells were then used to derive monthly averaged NLDAS2/observations ratios for solar radiation and wind, and the average monthly biases (i.e., NLDAS2—Observations) for air T. Finally, we apply the ratios and difference to the interpolated hourly NLDAS2 data on the other 1/16th grid cells to bias-correct the NLDAS2 data against the observational data, using the Bias-Correction Spatial Disaggregation (BCSD) method from Wood et al. (2004). This is the same forcing data set used in Zhu et al. (2020).

Meteorological forcing after 2015 used in this study is bilinearly interpolated from the bias corrected 1/8 grid hourly products simulated by the Regional Earth System Model (RESM) (Kraucunas et al., 2015). The RESM has been applied over North America at a 20 km grid resolution with lateral boundary conditions and sea surface T provided by CESM. Gao et al. (2014) evaluated the RESM historical simulation using observed T and P and found that simulations could reasonably capture the observed seasonal T and P and extreme P. The RESM hourly outputs in RCPs 4.5 and 8.5 were first downscaled and biased corrected to 1/8th degree against the NLDAS-2 forcing using the BCSD method, then bilinearly interpolate to 1/16 degree grid, and have been used in previous modeling studies in exploring impacts of land-based carbon mitigation strategies on regional-scale land-water-energy dynamics (Hejazi et al., 2015; Kraucunas et al., 2015). Specifically, a linear trend was fitted to the surface T time series between 2005 and 2099 using linear regression. Quantile mapping was applied to the residuals after removing the linear trend for each grid cell. This step was not needed for P since linear trends were not apparent for the projected P. The solar radiation fluxes were bias corrected by multiplying the long-term mean ratio against NLDAS2 data. Future atmospheric CO_2 concentration and N deposition rate is prescribed using data from CESM that correspond to each SSP-RCP scenario.

Table 1
Land Cover Types Over the Watershed

CLM5 land cover types	Area of the watershed (%)	Area of the cropland (%)
C3 unmanaged rainfed crop	10.5	22.3
C3 unmanaged irrigated crop	9.1	19.4
Corn	3.7	7.9
Winter wheat	13.9	29.6
Soybean	9.8	20.8
Natural vegetation	45	–
Urban	6.4	–
Lake	1.6	–

Land surface characteristics including land use and land cover (LULC) and soil texture are required to configuration the model. LULC are extracted from the 30 m CDL data set that is fully trained and assessed based on ground truth data and reclassified into CLM5 LULC categories. For example, corn, sweet corn, and double crop corn in the CDL map are reclassified as corn in the CLM5 categories; alfalfa, peas, and dry beans in the CDL types are reclassified as soybean. The areal coverages of the land cover types are shown in Table 1. The soil texture represented by percentage soil sand, soil clay, and organic density are derived from USDA Digital General Soil Map of the United States (USDA-NRCS, 2020). The soil hydraulic conductivity and porosity over the study domain range from 131 to 2,421 mm d^{-1} and 0.37 to 0.48 mm^3 mm^{-3}, respectively (Figure S1).

As described in Zhu et al. (2020), we configure CLM5 at a spatial resolution of 1 km that fully resolving the landscape heterogeneity, such as land covers and soil texture. There are total 4,656 grid cells over the watershed, while the domain only occupies a few grid cells in coarser resolution for typical global simulations (e.g., one grid cell at 1° × 1° resolution, 32 grid cells at 0.125° × 0.125° resolution). Given the highly nonlinear features of plant physiology and phenology our highly resolved simulations can better resolve landscape heterogeneity and its associated impacts on water, energy, and biogeochemical processes (B. Zhu et al., 2020). The model parameters are well calibrated and validated by comparing with observations from the flux tower (Figure 1) and MODIS products in terms of water, energy, and carbon fluxes, such as latent heat fluxes, soil moisture, ET, gross primary production (GPP), LAI in both natural, and agricultural ecosystems. It should be noted that there are some uncertainties of MODIS data in springs and winters due to cloud effects. The parameter values are kept the same for each experiment. We also turn on the irrigation model to provide sufficient available water for crop to grow when rainfall could be limited in the future and also add fertilization manually by applying a fixed fertilization rate in each year. The annual irrigation amount simulated by CLM5 is 79.6 mm yr^{-1} that close to the US Geological Survey (USGS) statistics at county scale. The model inputs of historical nitrogen fertilizer rates for corn and soybean are 16 gN m^{-2} yr^{-1} and 2 gN m^{-2} yr^{-1} based on the USDA recommendation for the study region.

2.4. Numerical Experiment Design

To evaluate the effects of climate, CO_2 concentration, and N availability, we conducted nine numerical experiments, one in the historical period as the baseline and eight under future scenarios. As shown in Table 2, a historical simulation (i.e., Hist) is performed from 1985 to 2014, using the initial condition generated by recycling historical forcing for 500 years until all water, carbon, and nitrogen states reach equilibrium. We use the following two criteria to determine equilibrium according to Huntzinger et al. (2013): (1) The mean interannual change in the simulated total ecosystem carbon stocks for consecutive years in the last 100 years must be less than 1 gC m^{-2} yr^{-1} for 95% of grid cells. (2) The 100 years trend in soil states (e.g., soil temperature and soil water) should keep stable and not be significantly different from zero ($\alpha = 0.05$) for at least 95% of grid cells. All eight future simulations span from 2015 to 2099. The first two simulations, named $S_{4.5}$ and $S_{8.5}$ hereinafter, only consider changes in meteorological variables only following RCP 4.5 and 8.5, respectively, while the CO_2 concentration, N deposition, and fertilization rates are kept the same

Table 2
Description of Numerical Experiments

Name	Forcing data set	Period	Climate	CO_2 concentration	N deposition	Fertilization
Hist	Observations	1985–2014	Yes	Yes	Yes	Yes
$S_{4.5}$	RCP4.5	2015–2099	Yes	Constant[a]	Constant[b]	Constant[c]
$S_{8.5}$	RCP8.5	2015–2099	Yes	Constant[a]	Constant[b]	Constant[c]
$S_{4.5+C}$	RCP4.5	2015–2099	Yes	Yes	Constant[b]	Constant[c]
$S_{8.5+C}$	RCP8.5	2015–2099	Yes	Yes	Constant[b]	Constant[c]
$S_{4.5+CN}$	RCP4.5	2015–2099	Yes	Yes	Yes	Constant[c]
$S_{8.5+CN}$	RCP8.5	2015–2099	Yes	Yes	Yes	Constant[c]
$S_{4.5+CNF}$	RCP4.5	2015–2099	Yes	Yes	Yes	Yes
$S_{8.5+CNF}$	RCP8.5	2015–2099	Yes	Yes	Yes	Yes

[a]CO_2 concentration is held constant at 2014 value of 401 ppm. [b]N deposition is held constant at 2014 value of 0.51 gN m^{-2} yr^{-1}. [c]Fertilization rates are held constant at value of 2 gN m^{-2} yr^{-1} for C3 crops and 16 gN m^{-2} yr^{-1} for C4 crops.

as those in the year 2014. $S_{4.5}$ and $S_{8.5}$ are referred to as "climate-only" simulations hereinafter. To examine the effects of increased CO_2, we perform another two simulations, referred to as $S_{4.5+C}$ and $S_{8.5+C}$, which are identical to $S_{4.5}$ and $S_{8.5}$ but forced by dynamic CO_2 concentrations from RCP4.5 and 8.5 instead of the constant value in year 2014, while the N deposition and fertilization rates are used for all years. Another two simulations, $S_{4.5+CN}$ and $S_{8.5+CN}$, are conducted by varying CO_2 concentration annually and N deposition monthly (https://svn-ccsm-inputdata.cgd.ucar.edu/trunk/inputdata/atm/datm7/). The projected N fertilization rates derived from Land use Harmanization 2 (LUH2) data set (Hurtt et al., 2020) are used as forcing in the last two experiments, $S_{4.5+CNF}$ and $S_{8.5+CNF}$, to understand the role of N fertilization. Given that the relative coarse resolution in the LUH2 data set (0.25-degree), and its slightly different initial fertilization rates over the study domain from our calibrated historical values, we applied the trend from the LUH2 data set to create the future fertilization usage. That is, the difference (Δ) between initial values of LUH2 and CLM5 was calculated as a constant and then added to the LUH2 trend to get the CLM5 fertilization rates under RCP4.5 and 8.5 scenarios (Equation 2).

$$\mathrm{CLM5}_{\mathrm{fert},i} = \mathrm{LUH2}_{\mathrm{fert},i} + \Delta \tag{2}$$

where the Δ for C3 crops is 1.2 gN m^2 yr^{-1}, for C4 crops is 2.5 gN m^2 yr^{-1}. The $\mathrm{CLM5}_{\mathrm{fert}}$ and $\mathrm{LUH2}_{\mathrm{fert}}$ are fertilization rates for CLM5 input value and LUH2 data set, respectively. i stands for each year from 2015 to 2099. All future simulations use the same initial condition obtained from the historical outputs by the end of year 2014.

In this study, we assume that LULC will not change significantly in the future by keeping LULC static based on the CDL data set in year 2014. Therefore, the nine experiments differ in climate, CO_2 concentration, N deposition, and N fertilization rates only.

2.5. Analyses

To isolate the effects of climate, CO_2, N deposition, and N fertilization rates on land surface processes, we gradually add one factor at a time in the simulations and analyze the differences between two simulations to quantify the influence of each factor. For each RCP, simulated variables from $S_{4.5}$ and $S_{8.5}$ in the future period (2070–2099) are compared to from those in the historical period (1985–2014) to understand the climate-only effect by the end of 21st century. By subtracting $S_{4.5}$ from $S_{4.5+C}$ or $S_{8.5}$ from $S_{8.5+C}$, we can isolate the influence of CO_2 increase from climate-only effects. Similarly, the N deposition effect is obtained by subtracting $S_{4.5+C}$ from $S_{4.5+CN}$ or $S_{8.5+C}$ from $S_{8.5+CN}$. The fertilization effect is obtained by subtracting $S_{4.5+CN}$ from $S_{4.5+CNF}$ or $S_{8.5+CN}$ from $S_{8.5+CNF}$. In this way, the responses of hydrological and biogeochemical terms to each individual factor are calculated. First, the N uptake and GPP of plants are analyzed by calculating

the annual value averaged from 2070 to 2099 in each scenario compared with averaged historical annual N uptake and GPP amount to examine the future biogeochemical dynamics in response to climate change. Since ET is one of the largest terms in the global land surface water budget (Bohn & Vivoni, 2016) and sensitive to climate changes (McKenney & Rosenberg, 1993), and closely related to the carbon and nitrogen cycles, we focus on ET changes over different land cover types and the watershed as a whole as well as its modulating factors in a changing climate to understand the linkage between the biogeochemical and hydrologic cycles. The cumulative frequency distributions (CDF) based on annual results for key hydrological variables (e.g., ET) are plotted to infer the differences among these scenarios. Furthermore, to investigate the dominate factor of cropland physiological and phenological responses on watershed hydrologic dynamics in the changing climate, we calculate the relationships between the biogeochemistry, hydrology budgets and physiological (e.g., stomatal resistance) and phenological features (e.g., leaf area index). For example, the relative differences in GPP, LAI, and N uptake (i.e., Δ GPP, Δ LAI, and Δ N uptake), and the changes in transpiration (Δ QVEGT) and Δ LAI and stomatal resistance (ΔR_s) are plotted and fitted using the linear regression method to quantify the relationships between land surfaces processes and plants physiology. To be consistent and comparable, the unit of each variable in Equation 3 is standardized and transformed to percentage.

$$\Delta X = \frac{X_{CO_2} - X}{X} \times 100\% \tag{3}$$

where X stand for the model outputs (e.g., N uptake, GPP, QVEGT, LAI, and R_s). X_{CO_2} indicate those budgets simulated by experiments with the CO_2 dynamics (e.g., $S_{4.5+C}$, $S_{4.5+CN}$, and $S_{4.5+CNF}$), and X are results from the $S_{4.5}$ and $S_{8.5}$, respectively. The changes of ET further perturb other water budgets dynamics (e.g., runoff, soil moisture, and groundwater), Therefore, the water balance equation (Equation 4) is used to evaluate the changes of water budgets amount over the watershed in the both historical and future scenarios:

$$\Delta \mathrm{TWS} = P + \mathrm{Irrig} - R_{\mathrm{over}} - R_b - \mathrm{ET} \tag{4}$$

where ΔTWS is the total water storage changes over the watershed, including surface water, soil moisture, and groundwater. P and Irrig are water inputs in the forms of P and irrigation, respectively. R_{over} is the surface runoff, R_b is the baseflow, and ET stands for evapotranspiration.

Finally, the water-use efficiency (WUE) (Equation 5) that represents a given level of biomass or grain yield per unit of water used by a specific crop (Hatfield et al., 2001) is calculated to identity the ability of the crop to adapt to climate change as follows:

$$\mathrm{WUE} = \frac{\mathrm{GPP}}{\mathrm{QVEGT}} \tag{5}$$

where WUE is the water-use efficiency, QVEGT and GPP stand for the transpiration and gross primary production for the given crop. To understand the changes of WUE under per ppm CO_2 concentration, we also calculate the ratio between WUE and CO_2 concentration (WUE/CO_2) to analyze the effects of future increasing CO_2 on WUE for crops.

3. Results

3.1. Changes in Environmental Factors

Changes in climate variables in terms of P, T, CO_2 concentration, atmospheric N deposition, and N fertilization rates over the UCPR watershed from 1985 to 2099 are shown in Figure 2. The annual P, T, and CO_2 concentration all show increasing trends, while the magnitudes of changes in RCP8.5 are higher than those in RCP4.5. The annual P will increase by the end of 21st century and the increase rates are 0.67 mm yr^{-1} for RCP4.5 and 0.63 mm yr^{-1} for RCP8.5. The seasonal variability of P is also changing with less rain during the growing season (June, July, and August) and more rainfall and snowfall in the winter (December, January, and February). By the end of the 21st century, mean annual T will be 4°C and 6°C higher than that of today

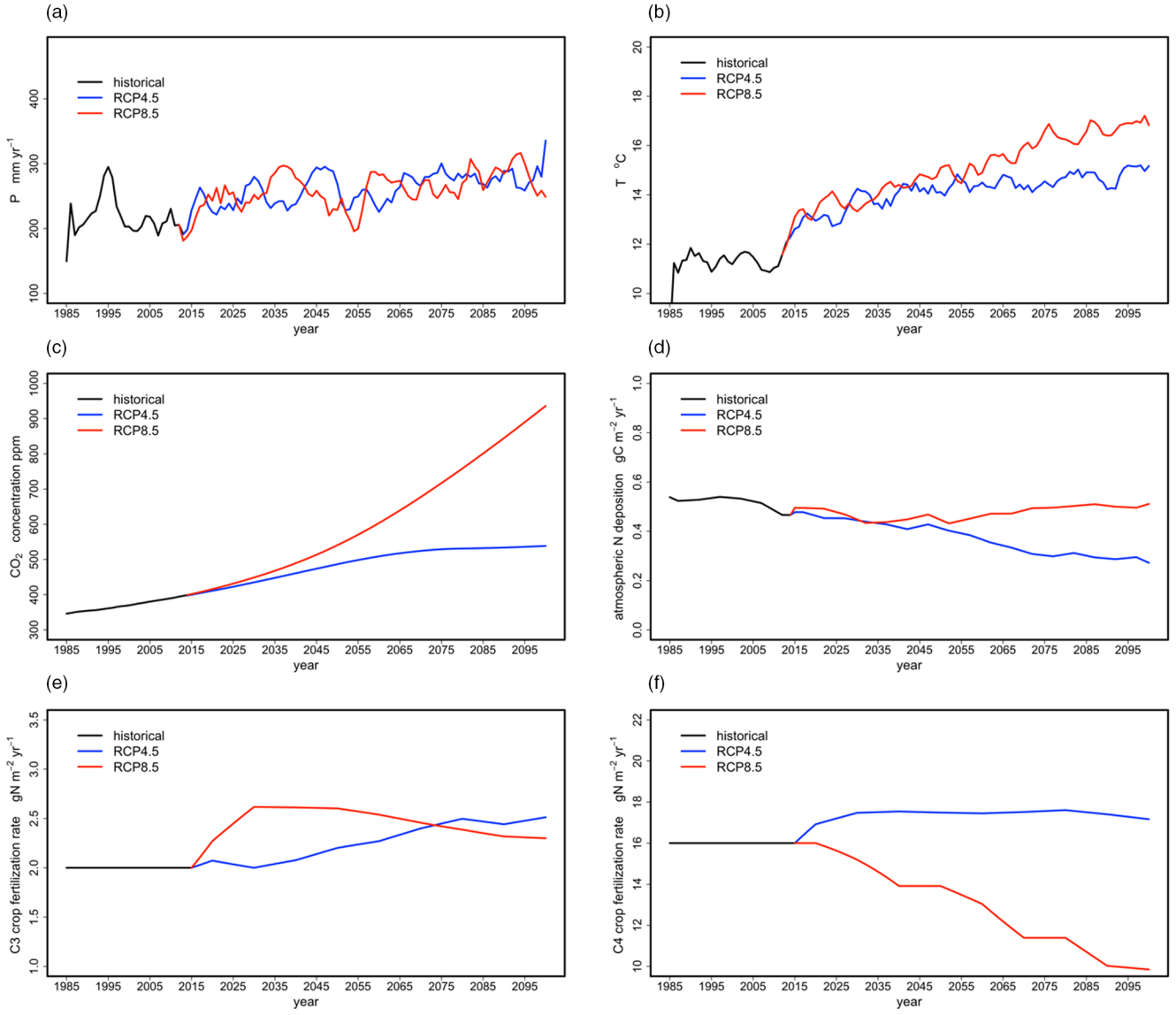

Figure 2. The changes in climate and environmental conditions: (a) annual precipitation with 5-year running mean, (b) annual temperature with 5-year running mean, (c) annual CO_2 concentration, (d) annual N deposition rate, (e) C3 crop fertilization rates, and (f) C4 crop fertilization rates.

for RCP4.5 and RCP8.5, respectively. The atmospheric CO_2 concentration will reach 538 and 935 ppm by the end of 21st century for RCP4.5 and RCP8.5, respectively, compared to 401 ppm in 2014. The atmospheric N deposition rate shows a decreased trend in RCP4.5 compared with its historical mean value (~0.51 gN m^{-2} yr^{-1}), while that in RCP8.5 remain stable over the UCPR watershed. The fertilization rate for C3 crops are relative stable in the future, and that for C4 crops slight increases by 2 gN m^2 yr^{-1} in RCP4.5 and decreases by 6 gN m^2 yr^{-1} in RCP8.5 because of the improved nitrogen use efficiency in the RCP8.5 projection of the LUH2 data set (Hurtt et al., 2020).

3.2. Biogeochemical Dynamics

3.2.1. GPP Changes

The atmospheric CO_2 is one major for terrestrial ecosystems (Le Quéré et al., 2009) being assimilated by plants through photosynthesis, and consequently influences the terrestrial carbon cycle. For the historical simulations, the annual GPP averaged over the watershed is 224 gC m^2 yr^{-1}, with higher GPPs for managed

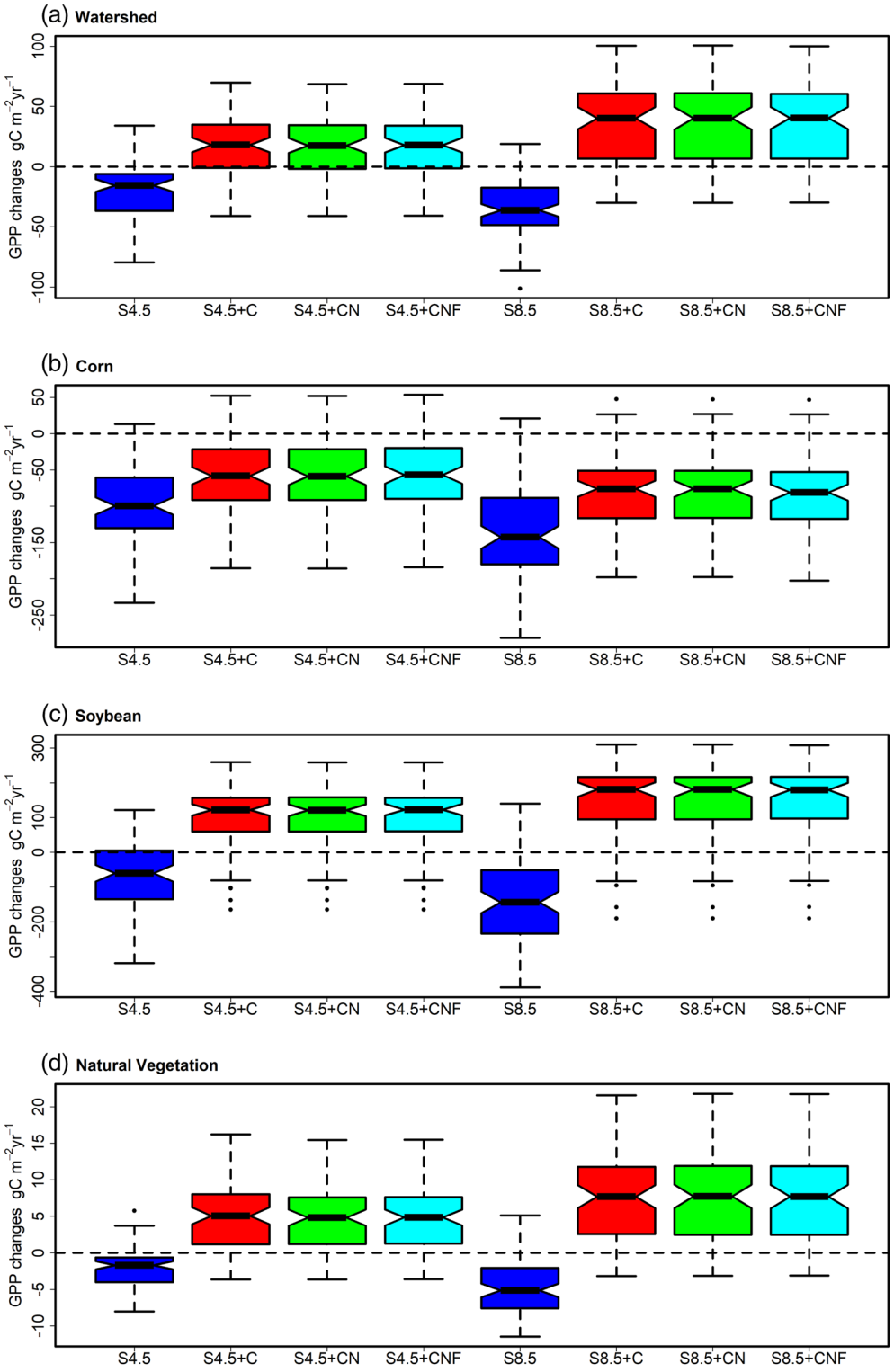

Figure 3. Changes in GPP in the period of 2070–2099 compared to their historical means over (a) the watershed (224 gC m^2 yr^{-1}), (b) corn (720 gC m^2 yr^{-1}), (c) soybean (782 gC m^2 yr^{-1}), and (d) natural vegetation (29.9 gC m^2 yr^{-1}). GPP, gross primary production.

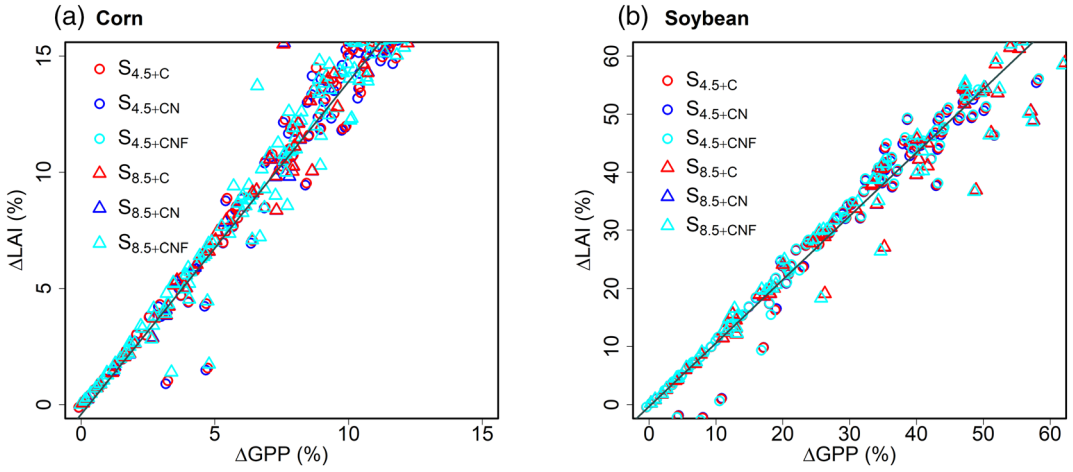

Figure 4. The relationships between GPP changes (Δ GPP) and LAI changes (Δ LAI) relative to climate-only scenarios for (a) corn and (b) soybean. GPP, gross primary production.

corn (720 gC m^2 yr^{-1}) and soybean (782 gC m^2 yr^{-1}), and a lower GPP in natural vegetation (29.9 gC m^2 yr^{-1}) because of lack of management practices such as irrigation and N fertilizers. As shown in the Figure 3, under the climate change only scenario from 2070 to 2099, GPP decreases slightly by 23.6 gC m^2 yr^{-1} and 48.9 gC m^2 yr^{-1} in $S_{4.5}$ and $S_{8.5}$ over the watershed due to a higher temperature and less precipitation during growing seasons.

When an elevated CO_2 concentration is considered, GPP increases significantly compared with the historical mean. The higher CO_2 concentration in $S_{8.5+C}$ results in a higher increase in annual GPP (~113 gC m^2 yr^{-1}) than that in $S_{4.5+C}$ (~56.9 gC m^2 yr^{-1}) over the watershed. For the irrigated crops (e.g., corn and soybean), the higher growing season temperature leads to a lower GPP, while the elevated CO_2 level could compensate such a reduction. For corn, simulated GPPs in $S_{4.5+C}$ and $S_{8.5+C}$ are 56.6 and 84.9 gC m^2 yr^{-1} higher than those in $S_{4.5}$ and $S_{8.5}$, respectively (Figure 3b). The effects of changing N deposition and fertilization rates are not as obvious as the CO_2 effect. Overall, simulated end-of-century GPP for corn is less than its historical value because the fixed N fertilization rate applied is not sufficient to support enhanced growth. For soybean, the combined effect of the CO_2 fertilization and its ability to fix soil mineral N results in net increases of 160 gC m^2 yr^{-1} in $S_{4.5+C}$ and 215 gC m^2 yr^{-1} in $S_{8.5+C}$ of simulated GPP, respectively. A higher CO_2 concentration also increases GPP of natural vegetation by 10.3 gC m^2 yr^{-1} (i.e., $S_{4.5+C} - S_{4.5}$) and 21.9 gC m^2 yr^{-1} (i.e., $S_{8.5+C} - S_{8.5}$). As a result, the combined effects of climate change and elevated CO_2 could amplify GPP, especially for croplands. Such a CO_2 fertilization effect is stronger in simulations under the RCP8.5 scenario than those under the RCP4.5 scenario as a result of its sharper increase in CO_2 concentration.

The enhanced photosynthesis also leads to higher leaf area indices over managed croplands. Figure 4 shows that, the relationship between Δ GPP and Δ LAI is highly linear. Following Equation 3, the Δ GPP ranges from 0% to 12% for corn, leading to increased Δ LAI ranging from 0% to 15%. For soybean, the highest Δ GPP reaches 50% that rises the Δ LAI for more than 60%. Therefore, CO_2 fertilization effect leads to increased LAI for both crops, which in turn further promote GPP.

3.2.2. N Uptake Changes

The terrestrial N carbon dynamics interact and modulate responses of ecosystems to elevated CO_2 (McGuire et al., 1995). The higher CO_2 concentration result in abundant carbon stored by plants which then provides the sufficient energy for plants to assimilate more N from soil, leading to higher photosynthesis capacities simulated in the LUNA and FUN models. During the historical period, the simulated N uptake averaged over the watershed is 3.32 gN m^2 yr^{-1}, with higher N uptake rates in corn (9.93 gN m^2 yr^{-1}) and soybean (11.8 gN m^2 yr^{-1}), and a lower rate in natural vegetation (0.34 gN m^2 yr^{-1}). Figure 5 shows changes in annual N uptake by comparing their simulated values in 2070–2099 to the historical mean.

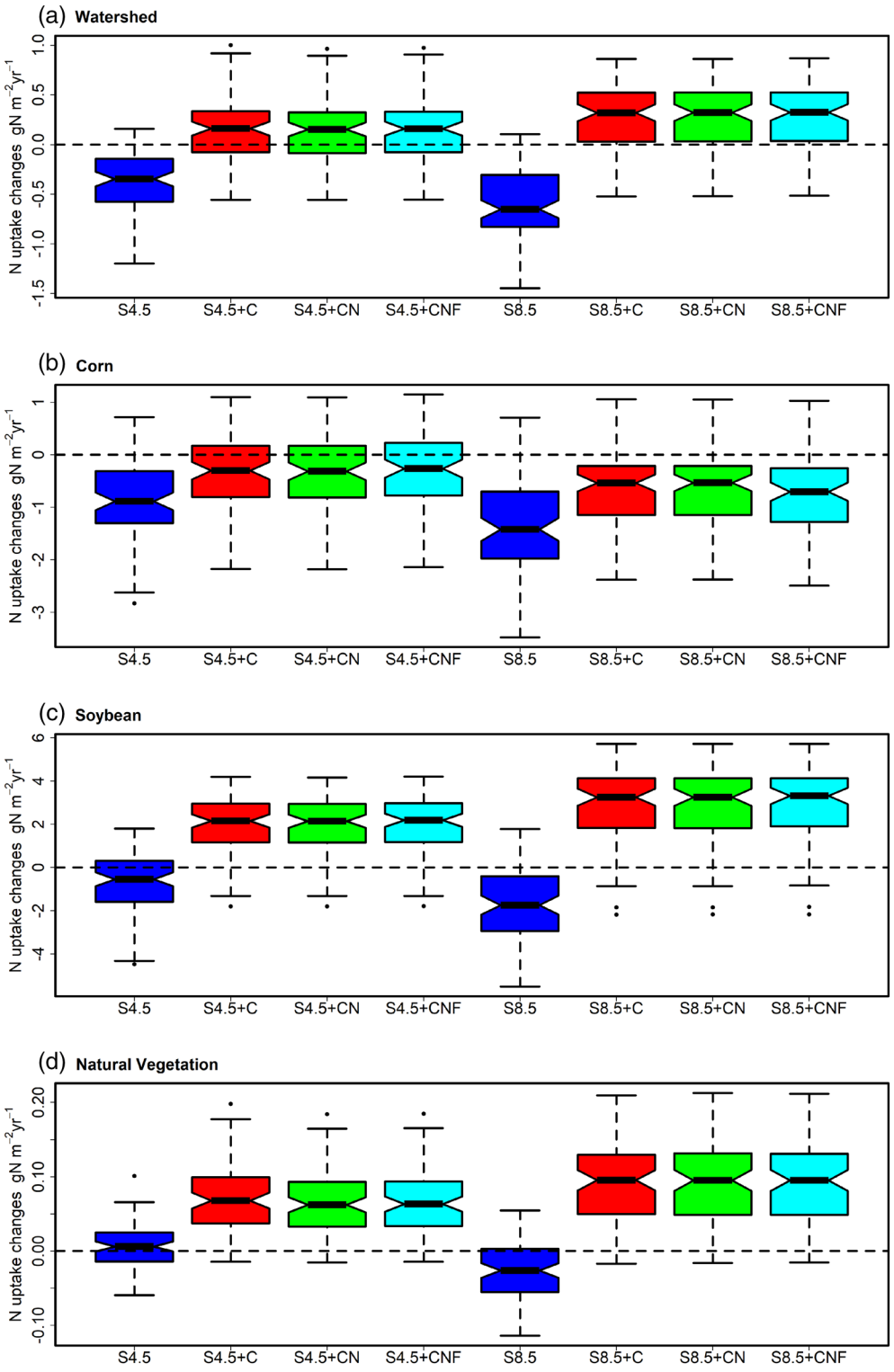

Figure 5. Changes in N uptake in the period of 2070–2099 compared to their historical means over (a) the watershed (3.32 gN m^2 yr^{-1}), (b) corn (9.93 gN m^2 yr^{-1}), (c) soybean (11.8 gN m^2 yr^{-1}), and (d) natural vegetation (0.34 gN m^2 yr^{-1}).

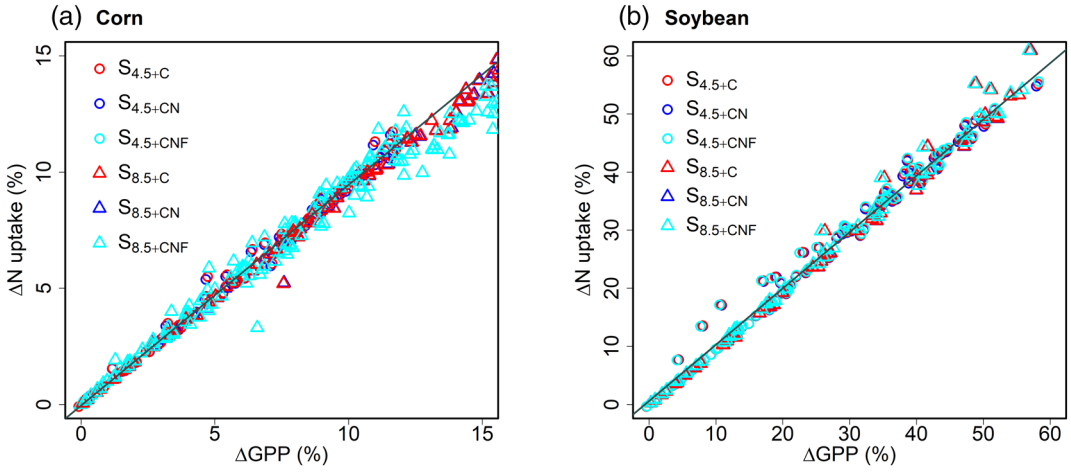

Figure 6. The relationships between changes in GPP and N uptake (Δ N uptake) relative to climate-only scenarios for (a) corn and (b) soybean. GPP, gross primary production.

Compared with the climate only simulations, the CO_2 fertilization effect enables corn to assimilate more N from the soil mineral pool by 0.80 gN m^2 yr^{-1} (9.2%) in $S_{4.5+C}$ and 1.13 gN m^2 yr^{-1} (14.5%) in $S_{8.5+C}$ compared to 8.70 gN m^2 yr^{-1} in $S_{4.5}$ and 7.78 gN m^2 yr^{-1} in $S_{8.5}$. The soybean can uptake more N by 3.95 gN m^2 yr^{-1} (36%) and 7.20 gN m^2 yr^{-1} (81%) in $S_{4.5+C}$ and $S_{8.5+C}$ compared to 10.7 gN m^2 yr^{-1} and 8.86 gN m^2 yr^{-1} in S4.5 and S8.5, respectively. When the continuous decreasing N deposition trend is accounted for in $S_{4.5+CN}$, N uptake only increases by 0.78 gN m^2 yr^{-1} and 3.92 gN m^2 yr^{-1} for corn and soybean than climate-only simulations, respectively. The simulated N uptake in $S_{8.5+CN}$ stays at the same level as that in $S_{8.5+C}$ for both crop types because of the stable N deposition trend under the RCP8.5 scenario. N uptake of natural vegetation is also enhanced under an elevated CO_2 concentration (Figure 5d). Compared to $S_{4.5}$ and $S_{8.5}$, the higher fertilization rates for corn lead to the increased N uptake by 0.83 gN m^2 yr^{-1} in $S_{4.5+CNF}$, and only 0.97 gN m^2 yr^{-1} increased N uptake are simulated in $S_{8.5+CNF}$ due to the decreased fertilization rates for RCP8.5 scenario. The effects of fertilization are not obvious over soybean-covered region because its fertilizer application rate stays stable. The changes in N uptake can further propagate to other N cycling processes in the terrestrial environment, such as denitrification and mineralization. For example, by the end of the century, compared with the historical mean, the denitrification rate over corn decreases by 0.17 and 0.19 gN m^2 yr^{-1}, while the simulated mineralization rate over corn increases by 1.10 and 1.27 gN m^2 yr^{-1} in $S_{4.5+C}$ and $S_{8.5+C}$.

The leaf N availability is the key element for photosynthesis. As shown in Figure 6, for both corn and soybean, strong linear relationships exist between Δ N uptake and Δ GPP, indicating that N uptake by plants increases with elevated CO_2 to meet photosynthesis requirements of the crops. Therefore, it is necessary to consider N dynamics when assessing impacts of future climate change.

3.3. Hydrologic Dynamics

The changes in biogeochemical cycle can fundamentally alter hydrologic cycle for both crops and natural vegetation through changes in vegetation phenology (e.g., LAI) and physiology (e.g., stomatal resistance) which connects the water transport among soil, plants, and atmosphere (Betts et al., 1997; Bounoua et al., 2010). The stomatal resistance is affected by both CO_2 concentration and photosynthesis (Equation 1), which is determined by the GPP and N availability of plants. The LAI is highly related to the GPP (Figure 4). From the perspective of physiology, both stomatal resistance and LAI control transpiration. Therefore, ET would be significantly perturbed when the carbon and nitrogen budgets are changed.

3.3.1. Changes in ET

As shown in Table 3, compared with the historical mean (254 mm yr^{-1}), annual ET over the UCPR watershed will increase by 37.1 mm yr^{-1} in $S_{4.5}$ and 30.0 mm yr^{-1} in $S_{8.5}$ by the end of the 21st century. The

Table 3
Annual evapotranspiration (ET) Changes Relative to Historical Mean

Hist mean (mm yr^{-1})		Future mean (mm yr^{-1})							
	Hist	$S_{4.5}$	$S_{4.5+C}$	$S_{4.5+CN}$	$S_{4.5+CNF}$	$S_{8.5}$	$S_{8.5+C}$	$S_{8.5+CN}$	$S_{8.5+CNF}$
Watershed	245	282 (37.1)	285 (40.2)	285 (40.0)	285 (40.0)	275 (30.0)	274 (28.7)	274 (28.7)	274 (28.6)
Corn	428	441 (13.1)	416 (− 11.5)	416 (− 11.6)	416 (− 11.4)	429 (1.63)	366 (− 62.4)	366 (− 62.4)	366 (− 63.1)
Soybean	507	536 (28.7)	563 (56.4)	563 (56.2)	563 (56.2)	490 (− 17.1)	514 (7.08)	514 (7.10)	514 (7.10)
Natural vegetation	150	188 (38.4)	189 (39.5)	189 (39.4)	189 (39.4)	395 (37.6)	397 (39.4)	397 (39.4)	397 (39.4)
Others (e.g., wheat, urban)	271	310 (39.7)	312 (41.8)	312 (41.5)	312 (41.5)	306 (35.5)	304 (33.7)	304 (33.7)	304 (33.7)

natural vegetation and unmanaged crops contribute the most ET increases over the watershed. The increase in atmospheric CO_2 concentration in the dynamic climate and CO_2 simulations ($S_{4.5+C}$ and $S_{8.5+C}$) could further elevate ET by 3.1 mm yr^{-1} and decline by 1.3 mm yr^{-1} (Table 3) compared to their respective climate-only simulations (i.e., $S_{4.5}$ and $S_{8.5}$). Variations in plant physiological traits lead to different responses of crop transpiration to changes in climate and ambient CO_2 concentration. For corn, compared with the climate-only simulations, the elevated CO_2 concentration leads to decreases in annual ET by 24.6 mm yr^{-1} and 64.0 mm yr^{-1} in $S_{4.5+C}$ and $S_{8.5+C}$ respectively. By contrast, ET from soybean increases by 27.7 and 9.98 mm yr^{-1} in $S_{4.5+C}$ and $S_{8.5+C}$ respectively. ET from natural vegetation in all future simulations with or without changes in CO_2 concentrations or N deposition remain close to each other, indicating the dominant control of climate trend on natural ecosystems. Since the N deposition rate show a slight declining trend in the RCP4.5 scenario so that less N is available for plant uptake, ET over the watershed in $S_{4.5+CN}$ is ~0.2 mm yr^{-1} lower than that $S_{4.5+C}$. The effect of changes in N deposition is not as significant as that of CO_2 concentration, because the atmospheric N deposition is only one source of external N input. The increased fertilization rates of RCP4.5 scenario result in higher ET by 0.2 mm yr^{-1} over corn from $S_{4.5+CNF}$ than $S_{4.5+CN}$,

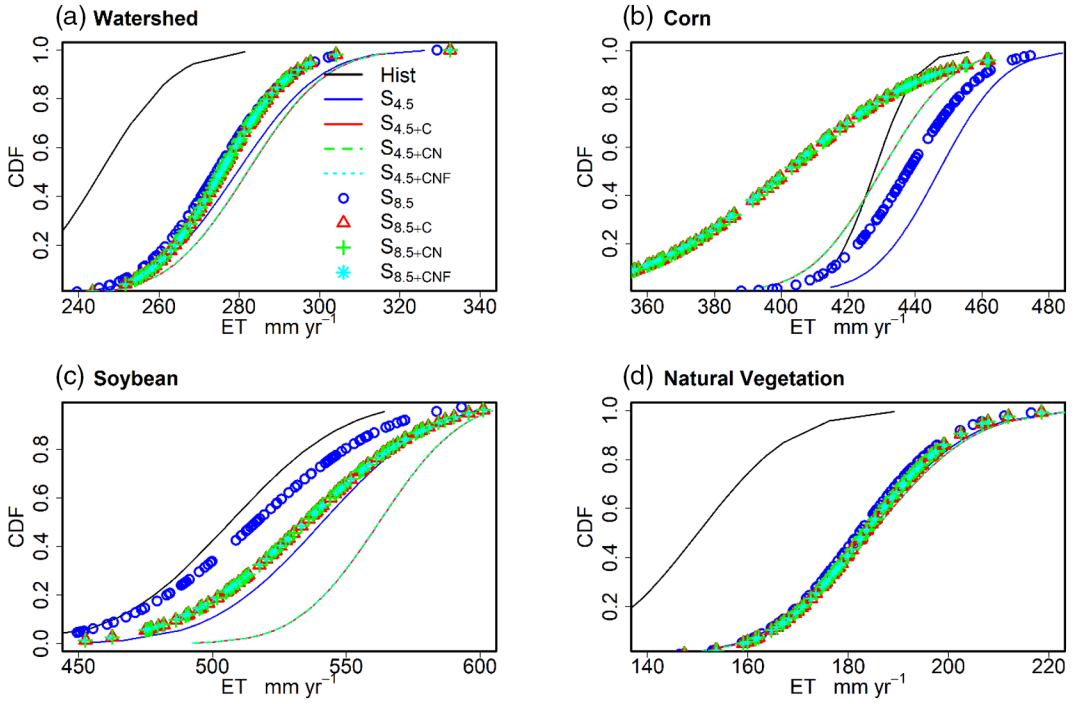

Figure 7. The CDFs for annual ET in response to historical and future climate for (a) the watershed, (b) corn, (c) soybean, and (d) natural vegetation. CDF, cumulative frequency distributions; ET, evapotranspiration.

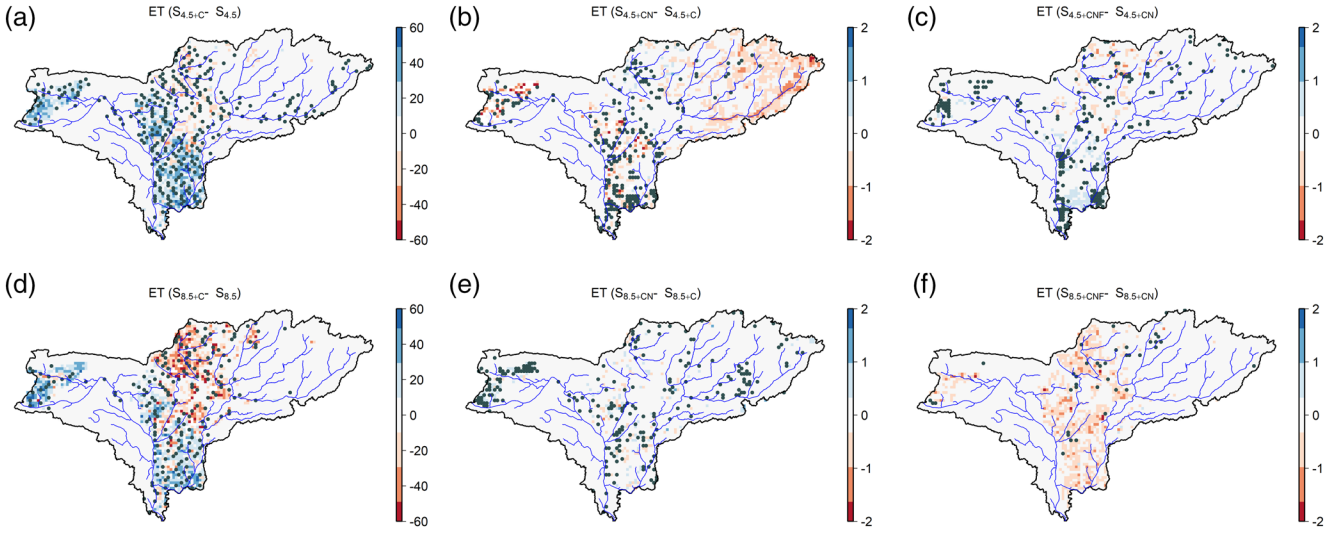

Figure 8. The spatial distributions of ET changes (mm yr^{-1}) with the effects from CO_2 concentration, N deposition, and N fertilization rates for RCP4.5 (a–c), and RCP8.5 (d–f). The black dots indicate the grid cells with significant changes in ET ($p < 0.05$). ET, evapotranspiration.

while lower ET by 0.7 mm yr^{-1} from $S_{8.5+CNF}$ than $S_{8.5+CN}$ are simulated because of the decreased fertilization rates of RCP8.5 scenario.

Figure 7 shows the CDFs of simulated annual ET in the period of 2070–2099 averaged over the watershed. For corn (Figure 7b), while the higher projected T in $S_{4.5}$ and $S_{8.5}$ pushes the upper bounds of ET to higher values, elevated CO_2 concentrations lead to decreases in ET in all other future simulations. The magnitudes of decreases in ET under RCP8.5 are more significant than those under RCP4.5. For soybean (Figure 7c), climate changes could either enhance or limit ET as evidenced by the general increase in $S_{4.5}$ and the general decrease in $S_{8.5}$, while CO2 fertilization in general elevate ET on top of climate change, with a higher sensitivity in lower percentiles. The CDFs of simulated future ET from natural vegetation are mostly overlapping but ET is generally higher than that in the historical distribution (Figure 7d), indicating the dominant effect of climate on ET, and a low sensitivity of natural vegetation to elevated CO_2 and N deposition. Spatially, when accounting for the higher CO_2 concentration, ET overwhelmingly increases over soybean (Figures 8a and 8d) compared with climate-only scenarios, with a maximum increase of more than 60 mm yr^{-1} during 2070–2099. Figures 8b and 8e show the spatial distribution of N deposition effects on ET. Due to lower N deposition rates in $S_{4.5+CN}$, ET decreases slightly over croplands, but does not change much in $S_{8.5+CN}$ compared to that in $S_{8.5+C}$. The changes in fertilization rates only slightly affect the ET over managed crops (Figures 8c and 8f). Overall, the ET responses to N availability are not as obvious as that to elevated CO_2 concentration.

In CLM5, ET is calculated as the sum of vegetation transpiration (QVEGT), canopy evaporation (QVEGE), and soil evaporation (QSOIL). Figure 9 shows changes in ET components. Compared to those in the historical period, due to higher precipitation during early spring when the LAI for natural vegetation and crops are low, averaged QSOIL over the watershed (Figure 9a) in the period of 2070–2099 increases by ~40 mm yr^{-1} in both $S_{4.5}$and $S_{8.5}$ simulations on top of the historical mean of 135 mm yr^{-1}. QVEGE increases slightly because the higher LAI allows for more canopy interception. However, the changes in QVEGT show different patterns in corn (Figure 9b) and soybean (Figure 9c). Under the climate-only scenarios (i.e., $S_{4.5}$ and $S_{8.5}$), QVEGT of both corn and soybean decrease, particularly in $S_{8.5}$ where a lower GPP (Figure 3) leads to higher stomatal resistance (Equation 1). When accounting for CO_2 effects, QVEGT declines by 21.9 and 59.2 mm yr^{-1} for corn and increased by 40.1 and 43.9 mm yr^{-1} for soybean under RCP4.5 (i.e., $S_{4.5+C}$, $S_{4.5+CN}$, $S_{4.5+CNF}$) and 8.5 scenarios (i.e., $S_{8.5+C}$, $S_{8.5+CN}$, $S_{8.5+CNF}$) compared to their historical values of 259 (corn) and 381 mm yr^{-1} (soybean).

To investigate dominate factors modulating QVEGT when CO_2 effects are accounted for, we investigated the changes of LAI and stomatal resistance $\left(R_s\right)$ between the dynamic climate + CO_2 and climate-only scenar-

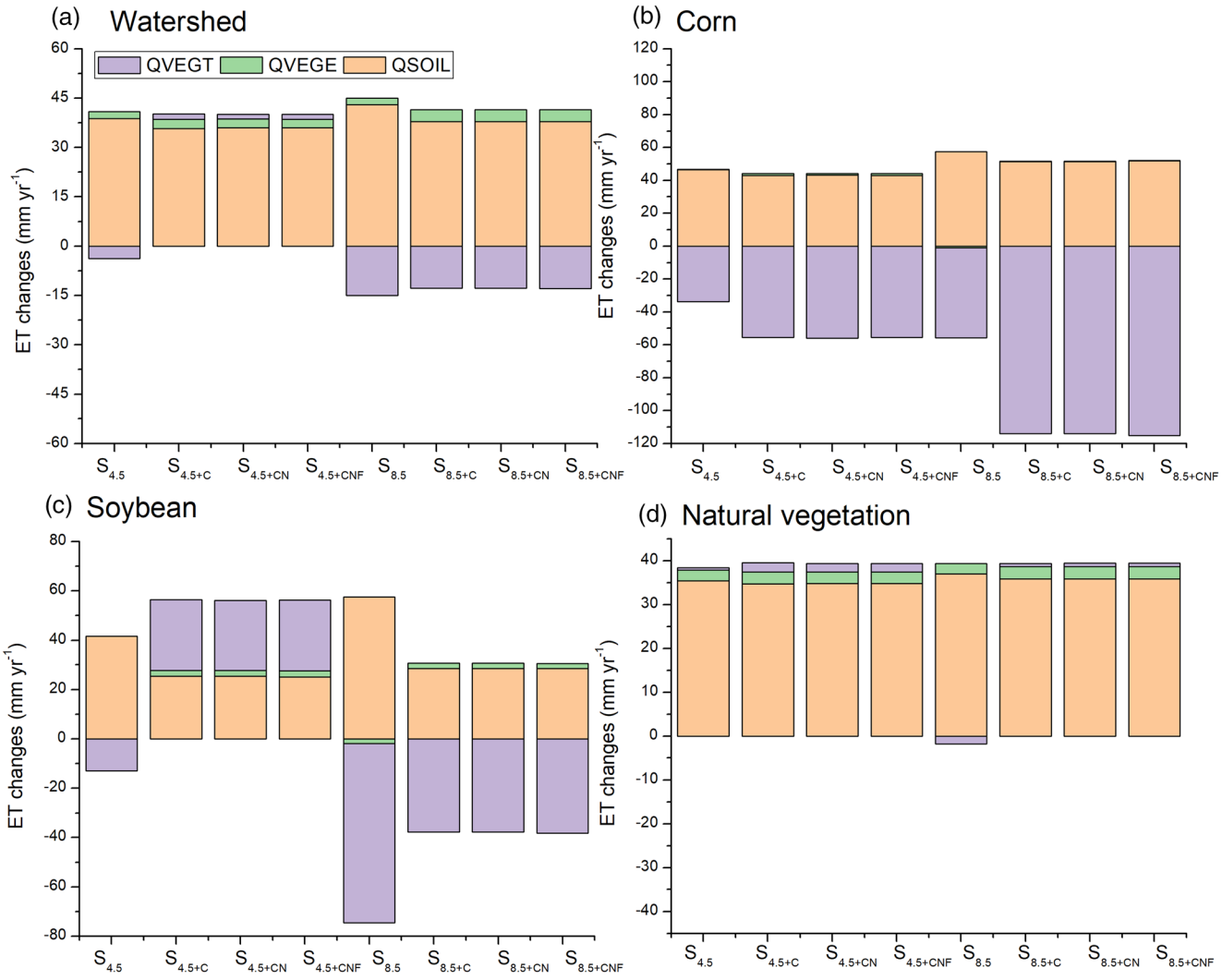

Figure 9. The changes of ET components-QVEGT, QVEGE, and QSOIL compared to their historical means over (a) watershed (102, 7.66, 135 mm yr^{-1}), (b) corn (259, 11.5, 157 mm yr^{-1}), (c) soybean (381, 12.8, 113 mm yr^{-1}), and (d) natural vegetation (15.3, 8.28, 126 mm yr^{-1}). The numbers indicate historical mean values of QVEGT, QVEGE, and QSOIL, respectively. The *x*-axis is the eight future scenarios. ET, evapotranspiration.

ios for corn and soybean, as shown in Figure 10 and Table 4. For corn, the regression coefficients of ΔR_s is higher than that of ΔLAI, indicating stronger modulation of R_s on QVEGT compared to that of LAI (Figure 10a). For RCP8.5, despite that LAI of corn increases under elevated CO_2, due to the significant higher ΔR_s, both ΔLAI and ΔR_s have negative coefficients in the regression equation (Figure 10b), leading to a lower QVEGT for corn. Furthermore, the averaged ΔR_s for all RCP4.5 and 8.5 climate +CO_2 simulations is 40.1%, which is higher than the ΔLAI (18.3%). Therefore, lower QVEGT of corn is simulated when CO_2 concentration increases. For soybean, as shown in Figures 10c and 10d, the modulation of R_s on QVEGT is weaker than that of LAI as indicated by the higher coefficients of ΔLAI. Furthermore, the percentage change of ΔLAI (59.8%) for all RCP4.5 and 8.5 climate +CO_2 simulations is higher compared with that of ΔR_s (30.2%), suggesting a stronger indirect impact of LAI on QVEGT from soybean. For natural vegetation, both ΔLAI and ΔR_s are also increased due to the CO_2 fertilization effects (Table 4), and ΔLAI is slightly higher than ΔR_s, therefore leading to minor increases in QVEGT, but less than that in corn and soybean because of lack of irrigation. Overall, when accounting for elevated CO_2 concentration, QVEGT from corn is reduced as a result of the strong negative influence of stomatal conductance than that of LAI. QVEGT

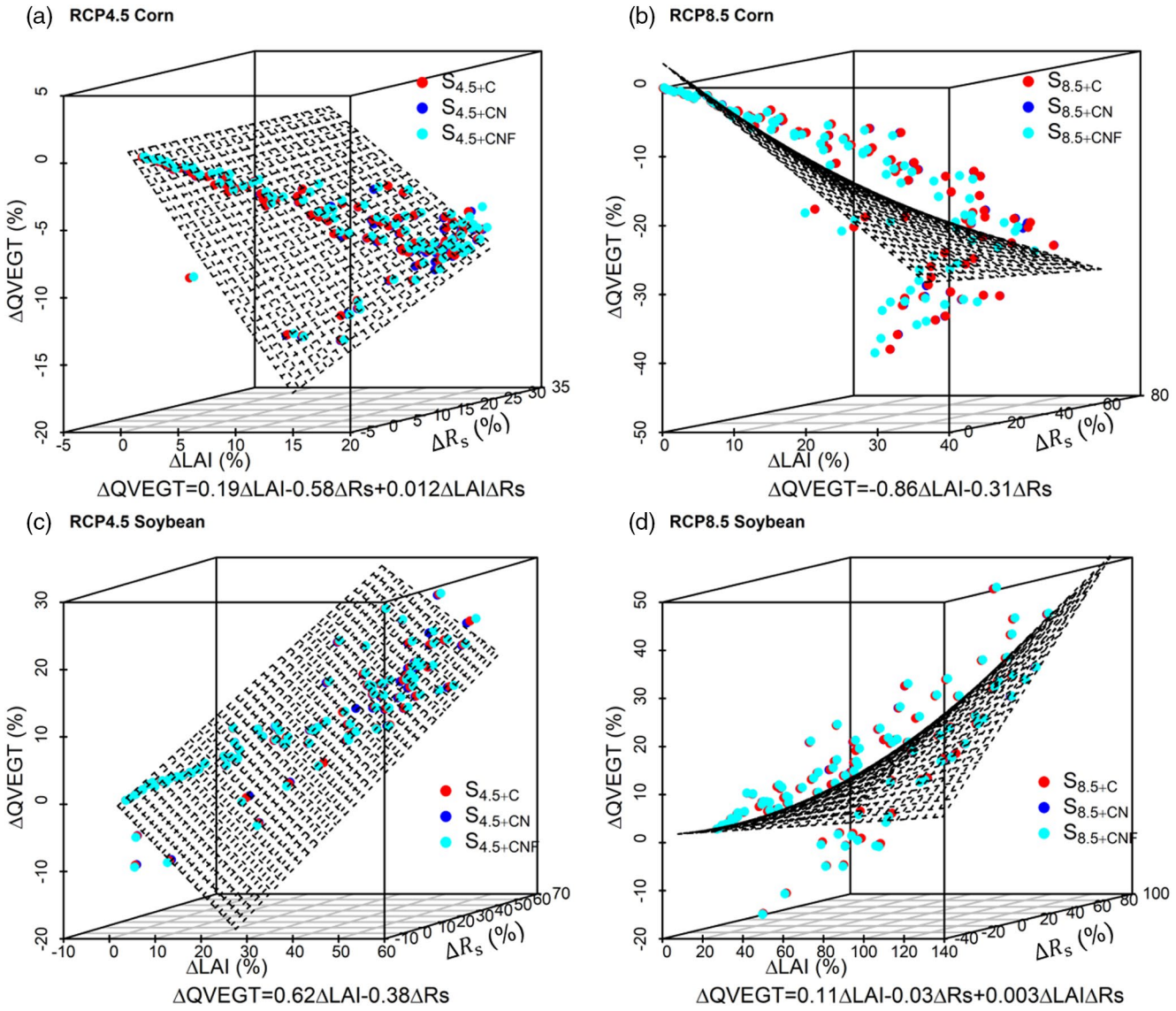

Figure 10. The relationships among transpiration changes ($^{\Delta}$ QVEGT) and LAI changes ($^{\Delta}$ LAI) and stomatal resistance changes ($^{\Delta}$ R_s) relative to climate-only scenarios for (a), (b) corn and (c), (d) soybean. Only significant terms ($p < 0.001$) are kept in the regression equations.

from soybean increases, however, because of the positive feedback between a higher rate of LAI increase and higher net photosynthesis.

Table 4
The Changes for LAI and Stomatal Resistance (Rs) Relative to Climate-Only Simulations

		$S_{4.5+C}$	$S_{4.5+CN}$	$S_{4.5+CNF}$	$S_{8.5+C}$	$S_{8.5+CN}$	$S_{8.5+CNF}$
ΔLAI (%)	Corn	12.8	12.5	12.6	24.0	24.0	23.6
	Soybean	38.5	38.2	38.3	81.4	81.4	81.4
	Natural vegetation	21.9	21.8	21.8	23.4	23.4	23.4
ΔR_s (%)	Corn	29.1	29.0	29.2	51.5	51.5	50.5
	Soybean	38.0	38.1	38.2	22.4	22.4	22.4
	Natural Vegetation	18.9	19.9	19.9	14.8	14.8	14.8

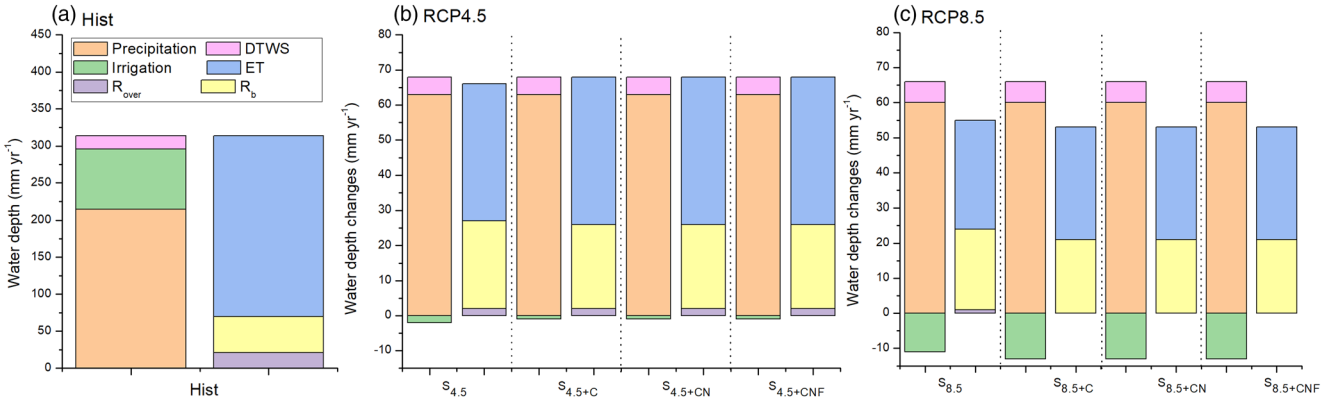

Figure 11. (a) Watershed-scale water balance during the historical period, (b) changes in water budget terms in simulations under the RCP4.5 scenario, and (c) changes in water budget terms in simulations under the RCP8.5 scenario in the period of 2070–2099.

3.3.2. Changes in Watershed-Scale Water Balance

The changes in ET can further propagate to other hydrologic terms, such as soil moisture (SM) and ground water table depth (ZWT). The higher soil evaporation in all future scenarios leads to decreases in soil moisture shown in Figure S2. Compared to the historical mean of 0.21 $mm^3\ mm^{-3}$, the simulated top 10-cm SM is around 0.20 $mm^3\ mm^{-3}$ over the watershed from $S_{4.5}$, while that simulated in $S_{8.5}$ is 0.18 $mm^3\ mm^{-3}$ because of the higher soil evaporation in $S_{8.5.}$ Changes in CO_2 concentration and N availability slightly decrease SM over corn by 0.0007 $mm^3\ mm^{-3}$ in $S_{4.5+CNF}$ and 0.0021 $mm^3\ mm^{-3}$ in $S_{8.5+CNF}$, and that over soybean by 0.0004 $mm^3\ mm^{-3}$ in $S_{4.5+CNF}$ and 0.0025 $mm^3\ mm^{-3}$ in $S_{8.5+CNF}$. This additional decrease in SM can be attributed to enhanced water uptake by roots as a result of CO_2 fertilization, leading to less soil moisture in the top soil layer. For groundwater depths underneath key land use cover types (Figure S3), shallower groundwater is simulated in the future (~8.36 m in $S_{4.5+CNF}$ and 8.37 m in $S_{8.5+CNF}$) relative to historical simulation (~8.45 m) over the watershed.

Figure 11a shows the water balance over the watershed in the historical period. *P* and irrigation are two major water inputs, and ET is the largest output term, followed by the R_b and R_{over}. Compared to the historical results, P increases by 63 mm yr^{-1} in RCP4.5 scenarios (Figure 11b), leading to a higher ET and runoff over the watershed. Since QVEGT originates from the root-zone soil moisture, and irrigation is calculated based on the root-zone soil moisture deficits, the two terms are strongly correlated. $S_{4.5+C}$ and $S_{4.5+CN}$ simulate higher QVEGT than $S_{4.5}$, consistent with the 2 mm yr^{-1} increase in irrigation amount over the watershed under the elevated CO_2 concentration. *P* increases by 61 mm yr^{-1} in RCP8.5 (Figure 11c), resulting in a higher ET and runoff relative to historical simulation, although smaller than those in RCP4.5. Compared to its historical value, irrigation in $S_{8.5}$ declines by 11 mm yr^{-1} because of lower QVEGT over the corn and soybean. When accounting for the CO_2 effects, irrigation over the watershed declines by 13.6 mm yr^{-1}, due to the significantly decrease in QVEGT of corn. Despite the decrease in irrigation amount, ZWT becomes shallower, contributed by increases in *P* that recharge groundwater in all future scenarios. Even though ET over irrigated croplands (e.g., corn and soybean) has been shown to be sensitive to CO_2 concentration that could potentially affect recharge to groundwater, the changes of ZWT over corn and soybean fields when accounting for the CO_2 effects are insignificant because irrigation water acts as a buffer to sustain aquifer storage by recharging it through percolation.

The ET and irrigation are two major water budgets that are highly related to LULC. Figure 12 shows the contributions of each land use type to the changes in ET and irrigation over the watershed over the period of 2070–2099 relative to historical simulation. For climate-only scenarios (e.g., $S_{4.5}$, $S_{8.5}$), ET increases are mainly contributed by natural vegetation, C3 crops, and urban as a result of increased P in combination with their relatively large areal coverages (45%, 19.6%, and 6.4%). Corn and soybean, which only account for around 4% and 10% of the total drainage area, have little contribution to the increases in ET. However, when an elevated CO_2 concentration is accounted for in addition to climate change, ET can be positively or negatively influenced depending on the scenarios under consideration. Under RCP4.5, a higher ET (i.e.,

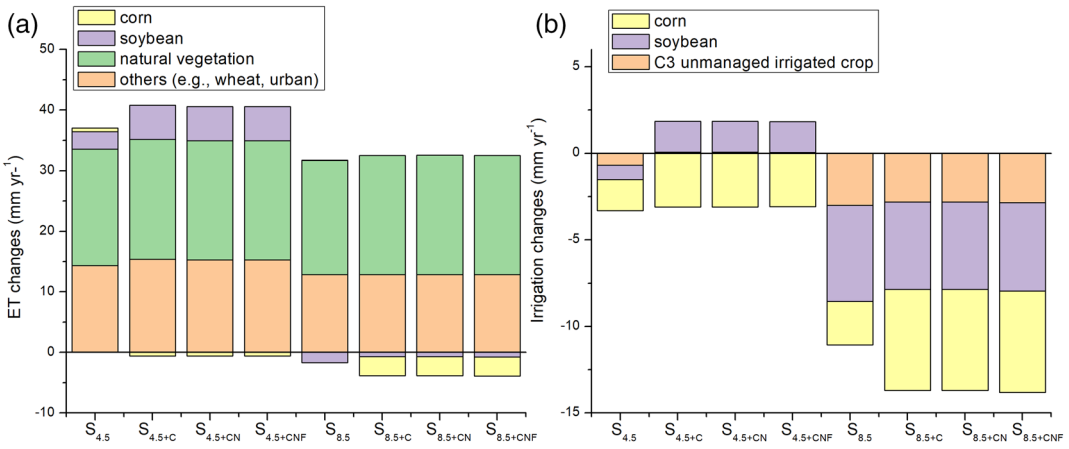

Figure 12. The contributions of each land use type to (a) changes in ET and (b) changes in irrigation over the watershed compare to their historical values. ET, evapotranspiration.

$ET_{S4.5+C} - ET_{S4.5} = 3.1$ mm yr^{-1}) over the watershed is simulated, contributed by a significant increase in soybean ET (~2.78 mm yr^{-1}). In comparison, under RCP8.5, a lower ET over the watershed (i.e., $ET_{S8.5+C} - ET_{S8.5} = 1.34$ mm yr^{-1}) is simulated because of the decreased ET from corn (~3.2 mm yr^{-1}) and increased ET from soybean (~1.0 mm yr^{-1}). Simulated ET in $S_{4.5+CN}$ or $S_{4.5+CNF}$ and $S_{8.5+CN}$ or $S_{8.5+CNF}$ are close to those in $S_{4.5+C}$ and $S_{8.5+C}$, because physiological and phenological responses in corn and soybean stay similar under the same CO_2 concentration trend when water and nutrient demands are met at least partially by irrigation and fertilization. Therefore, when accounting for CO_2 effects, changes in ET over the watershed can be strongly modulated by the physiological and phenological changes in corn and soybean as discussed in Section 3.2 in despite of their small areal coverages.

Figure 12b shows changes in irrigation over the watershed. Compared to the historical simulation, irrigation amounts of corn, soybean, and C3 unmanaged irrigated crop (e.g., pasture) simulated by $S_{4.5}$ and $S_{8.5}$ decrease with higher projected precipitation. When elevated CO_2 effects are accounted for, for RCP4.5 scenarios, although irrigation over corn decreases by 1.29 mm yr^{-1}, irrigation over soybean increases by 2.61 mm yr^{-1}. Combined with the limited increase of irrigation over the C3 unmanaged irrigated crop, irrigation amount over the watershed shows an overall increase of 2 mm yr^{-1}. For RCP8.5 scenarios, when accounting for the CO_2 fertilizer effects, irrigation over corn decreases significantly by -3.34 mm yr^{-1}, while

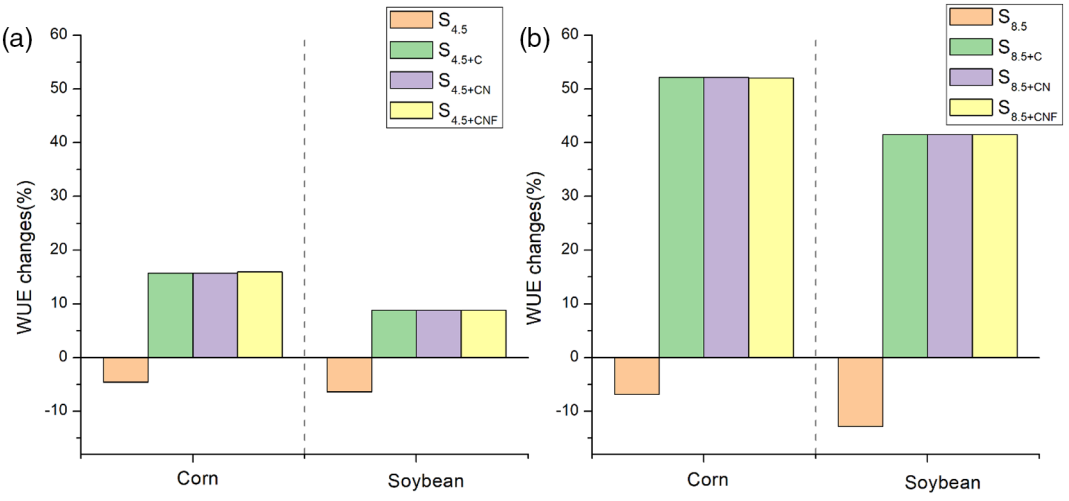

Figure 13. Changes in simulated WUE in the period of 2070–2099 compared to their historical means for (a) RCP4.5 and (b) RCP8.5. WUE, water-use efficiency.

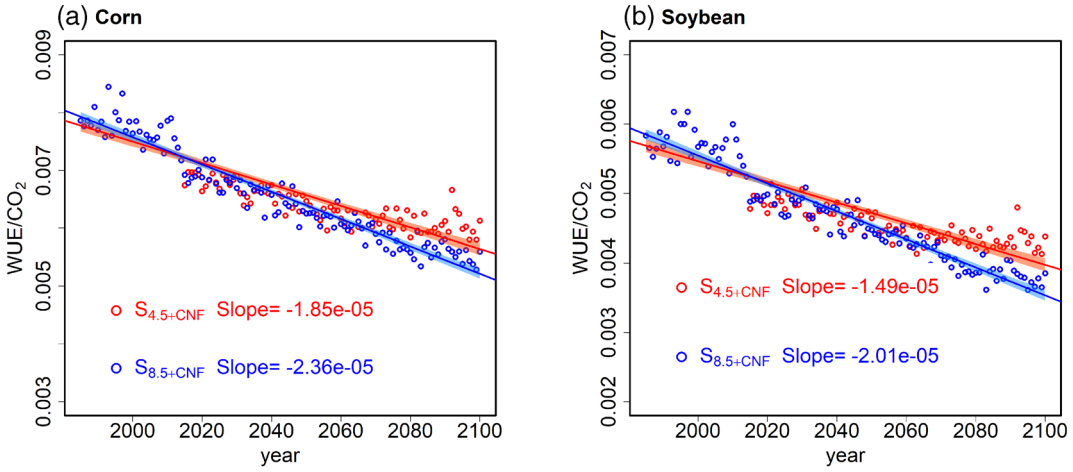

Figure 14. The changes of ratio between WUE and CO_2 concentration (ppm) from 1985 to 2099 for (a) corn and (b) soybean (shade areas are 95% confidence interval). WUE, water-use efficiency.

irrigation over soybean increases by 0.5 mm yr^{-1} ($S_{8.5+C} - S_{8.5}$), resulting in a lower total irrigation demand (~2.63 mm yr^{-1}) over the watershed under elevated CO_2 scenarios relative to climate-only scenario. Therefore, the expected elevated CO_2 concentration can impact watershed-scale water budget by modulating ET and irrigation over corn and soybean.

3.4. Water-Use Efficiency

WUE is an important index to link the carbon and hydrological cycles (Q. Zhu et al., 2011). Figure 13 shows changes in simulated future WUE for managed corn and soybean compared to those in the historical period. Under RCP4.5, WUEs for corn and soybean reduce by − 4.54% and − 8.61% in $S_{4.5}$ (Figure 8a), while the higher CO_2 concentration in $S_{4.5+C}$ leads to increases in WUE by 15.7% and 11.9% as a result of lower QVEGT of corn and higher GPP of soybean. Similarly, under RCP8.5 (Figure 13b), when accounting for CO_2 fertilization, WUEs increase in general. The changes of WUE of corn in $S_{8.5+C}$ and $S_{8.5+CN}$ (~52.1%) are significantly higher than its historical value, indicating its strong adaptation to future climate change by less water consuming. Despite that an elevated CO_2 concentration can enhance QVEGT from soybean, the more significant increase in GPP results in an increase in WUE in $S_{8.5+C}$ by almost 41.5% compared with that in the historical period. Meanwhile, since the N deposition rate slightly increases by the end of 21st century (Figure 2d), the simulated WUE for soybean in $S_{8.5+CN}$ in which the N deposition effect is accounted for is the highest than those from other experiments, although only 0.01% increase relative to $S_{8.5+C}$, suggesting that both factors could benefit productivity with less water consumption in the future. The increased N fertilization inputs from $S_{4.5+CNF}$ lead to higher WUE by 0.07% over corn and 0.03% over soybean than from $S_{4.5+CN}$. By contrast, the WUE of $S_{8.5+CNF}$ is decreased by 0.32% over corn and kept same over soybean compared to $S_{8.5+CN}$.

We calculate the changes in WUE per CO_2 concentration (WUE/CO_2) from $S_{4.5+CNF}$ and $S_{8.5+CNF}$ for corn and soybean over the periods of 1985–2099 (Figure 14). It is clear that the WUE per ppm of CO_2 decreases with increasing CO_2 concentrations in general. Therefore, although the WUE of soybean increases in the future as shown in Figure 14, decreasing trends of WUE/CO_2 ratio in $S_{4.5+CNF}$ and $S_{8.5+CNF}$ in Figure 14b suggest that the increase rate of WUE is slowing down and the CO_2 driven gains in WUE is diminishing as CO_2 concentration increases (Adams et al., 2020).

4. Conclusions and Future Work

Climate change can impact watershed hydrology and biogeochemical cycling. To investigate such effects, we applied the calibrated CLM5 over a typical semiarid watershed, the Upper-Columbia and Priest Rapids watershed, located in the Pacific Northwest. We considered changes in climate variables (e.g., P and T) and

associated changes in atmosphere CO_2, N deposition, and fertilization rates in a set of numerical experiments spanning from 2015 to 2099. Dominant plant functional types, such as soybean, corn, and natural vegetation, are fully resolved in the model and illustrated diverse responses to climate change. The elevated CO_2 directly increases GPP, which will in turn increase carbon stock and allocation to LAI. The higher GPP also leads to increase plants N uptake rates that provide additional leaf N to enhance photosynthesis. As a result, the changes in stomatal resistance and increased LAI that affect ET. The changes in ET eventually influence other hydrologic budget terms, such as soil moisture, groundwater table depth, and irrigation demand over the watershed. The major conclusions from this study are as follows:

1. The CO_2 fertilization effect could compensate the reduction in GPP as seen in the climate-change only scenarios. The higher GPP also leads to the increased LAI over croplands. Meanwhile, the increased GPP tends to demand more N and thus promote N uptake from soil mineral to improve photosynthesis capacity, while the decline in N deposition and fertilization rates trend could decrease the available N amount in the ecosystem
2. By comparing simulations between the historical and future simulations, we find that the natural vegetation contributes to more than 50% in watershed ET changes under climate-only scenario. By contrast, the croplands are more sensitive to elevated CO_2 concentrations than natural vegetation. The increase in CO_2 lower the ET over corn by 24.5 mm yr^{-1} under RCP4.5, and by 64.0 mm yr^{-1} under RCP8.5, respectively by the end of the century. Meanwhile, it enhances ET over soybean by 27.7 mm yr^{-1} under RCP4.5 and 9.98 mm yr^{-1} under RCP8.5. The main contributor of the opposite ET trends between soybean and corn is the differences in QVEGT. The effect of changes in N deposition and fertilization rates on the hydrological cycles is limited based on our study, which can be attributed to the modest changes in projected N deposition and fertilization, and that the fertilization use efficiency is not considered in the model
3. In general, the elevated CO_2 concentration level results in a reduced stomatal aperture (Ainsworth & Rogers, 2007), leading to less vapor through the leaf and therefore a reduction in QVEGT. However, increases in net photosynthesis and consequently larger LAIs under a higher CO_2 concentration environment could rise the QVEGT (Pritchard et al., 1999). The increase of QVEGT over soybean can be attributed to phenological (i.e., changes in LAI) factors as a higher positive coefficient between $\Delta\mathrm{QVEGT}$ and $\Delta\mathrm{LAI}$ are found, while QVEGT over corn field is declining contributed mainly by the physiological factor (i.e., changes in stomatal resistance) as a result of higher negative coefficient between $\Delta\mathrm{QVEGT}$ and ΔR_s under elevated CO_2. The changes in $\Delta\mathrm{LAI}$ is slightly higher than ΔR_s for natural vegetation, resulting in minor increases in QVEGT
4. The top 10-cm soil moisture decreases in response to a higher soil evaporation and root uptake capability, while no obvious changes are exhibited for groundwater because the increase in *P*. The changes of irrigation are directly affected by the QVEGT, which are decreased for corn and increased for soybean when accounting for the CO_2 fertilization effects. The changes in water budget terms over the watershed can be strongly modulated by physiological and phenological changes in corn and soybean in response to expected changes in greenhouse gas concentrations and atmospheric composition. The WUE for both corn and soybean are higher than climate-only scenario, while the CO_2 driven gains in WUE is diminishing as CO_2 concentration increases

Through high-resolution simulations that fully resolves land-scape heterogeneity over a semiarid watershed, we demonstrate that increased CO_2 concentration significantly influence terrestrial water and carbon cycling through modulating plant physiology and phenology. While earlier global scale studies (Betts et al., 1997; Levis et al., 2000; Pu & Dickinson, 2014) have demonstrated similar linkages between terrestrial carbon and water cycles, our study confirms that the natural vegetation and unmanaged crops are identified as the land types easily affected by climate change, and irrigated croplands (e.g., corn, soybean) can be the most sensitive land type to projected changes in elevated CO_2 concentration and fertilization as a result of their physiological and phenological responses, therefore dominate watershed-scale hydrologic responses when the CO_2 concentration is changing rapidly. According to Food and Agriculture Organization (FAO) report, the area of cropland over the globe is 1.5 billion ha accounting for 11% of globe's land surfaces (http://www.fao.org/3/y4252e/y4252e00.htm#TopOfPage). Therefore, it is crucial to parameterize crop-specific phenology and physiology in watershed-scale climate impact studies.

Our study provides comprehensive analysis of responses to climate change over a semiarid watershed and its key landscape component using CLM5 at a hyperresolution, which implicate the importance of representing the land surface and forcing data set heterogeneity, such as LULC, soil texture, and climate forcing, to improve model accuracy. Furthermore, our study could be a benchmark for regional agricultural and water resources management to better adapt to climate changes. For example, changes to crop management and types can be one of the main adaptation strategies needed for continued agricultural productivity. Alternatively, developing the crops with endosymbiotic nitrogen-fixing bacteria to supply their future N needs (Canfield et al., 2010) such as corn which has a higher WUE, is beneficial to improve food productivity and meet increasing human demand.

Further work is needed to address limitations in this study. First, we isolate the single effect by subtracting two simulations, but the climate effect can be interpreted as the joint impacts of changes in meteorological forcing and CO_2 concentration. Our analyses suggest that interaction effects are not significant in the scenarios explored in this study (results not shown). Nevertheless, such effects shall be explored in climate change impact studies due to uncertainties in future projected changes in different regions.

Second, land use and land cover change can strongly modify the watershed hydrologic budget, while we kept the land use and land cover to be the same in both historical and future simulations. We acknowledge that expansion of urban area and cropland are expected as a result of future population increase and consequent needs for food and energy (Schilling et al., 2008). Such potential changes necessitate further efforts to examine watershed responses to the combinations effects from land use change and climate change (DeFries & Eshleman, 2004).

Third, we note that although there are eight activated crop types in the CLM5, winter wheat, a typical crop type over the watershed, is not properly parameterized in the model. Winter wheat covers large areas in the US Great Plains (Weiss et al., 2003) and plays an important role in carbon cycling and land-atmosphere interactions (Lu et al., 2017). To represent wheat winter as well as other crop types (e.g., grapes, potatoes) in the CLM5 is necessary to better simulate cropland functions. Furthermore, irrigation and fertilization are as the only crop management practices in the model, while other practices such as tillage and residue management can further influence watershed hydrologic budget. These adaption strategies could be explored in future studies.

Data Availability Statement

The model input files, outputs, and driving scripts can be found online at https://doi.org/10.5281/zenodo.4086154.

Acknowledgments
This study was funded by the by the U.S. Department of Energy (DOE), Office of Biological and Environmental Research (BER), as part of BER's Subsurface Biogeochemical Research Program (SBR). This contribution originates from the SBR Scientific Focus Area (SFA) at the Pacific Northwest National Laboratory (PNNL). This research was also supported by the National Natural Science Foundation of China (NO. 41971030). We would like to acknowledge the Hanford Meteorological Station for sharing the observed meteorological variables used as inputs in this study.

References

Abdulla, F., Eshtawi, T., & Assaf, H. (2008). Assessment of the impact of potential climate change on the water balance of a semi-arid watershed. *Water Resources Management*, *23*(10), 2051–2068.

Adams, M. A., Buckley, T. N., & Turnbull, T. L. (2020). Diminishing CO_2-driven gains in water-use efficiency of global forests. *Nature Climate Change*, *10*, 1–6.

Ainsworth, E. A., & Rogers, A. (2007). The response of photosynthesis and stomatal conductance to rising [CO_2]: Mechanisms and environmental interactions. *Plant, Cell and Environment*, *30*(3), 258–270.

Ali, A. A., Xu, C., Rogers, A., Fisher, R. A., Wullschleger, S. D., Massoud, E. C., et al. (2016). A global scale mechanistic model of photosynthetic capacity (LUNA V1.0). *Geoscientific Model Development*, *9*(2), 587–606.

Betts, R. A., Cox, P. M., Lee, S. E., & Woodward, F. I. (1997). Contrasting physiological and structural vegetation feedbacks in climate change simulations. *Nature*, *387*(6635), 796–799.

Bohn, T. J., & Vivoni, E. R. (2016). Process-based characterization of evapotranspiration sources over the North American monsoon region. *Water Resources Research*, *52*(1), 358–384. https://doi.org/10.1002/2015WR017934

Bounoua, L., Hall, F., Sellers, P., Kumar, A., Collatz, G., Tucker, C., & Imhoff, M. (2010). Quantifying the negative feedback of vegetation to greenhouse warming: A modeling approach. *Geophysical Research Letters*, *37*(23), L23701. https://doi.org/10.1029/2010GL045338

Butcher, J. B., Johnson, T. E., Nover, D., & Sarkar, S. (2014). Incorporating the effects of increased atmospheric CO_2 in watershed model projections of climate change impacts. *Journal of Hydrology*, *513*, 322–334.

Canfield, D. E., Glazer, A. N., & Falkowski, P. G. (2010). The evolution and future of Earth's nitrogen cycle. *Science*, *330*(6001), 192–196.

Chen, B., & Liu, Z. (2016). Global water vapor variability and trend from the latest 36 year (1979 to 2014) data of ECMWF and NCEP reanalyses, radiosonde, GPS, and microwave satellite. *Journal of Geophysical Research: Atmospheres*, *121*(19), 11442–11462. https://doi.org/10.1002/2016JD024917

Dalton, M. M., & Mote, P. W. (2013). *Climate change in the northwest*: Springer.

Dawson, T. P., Perryman, A. H., & Osborne, T. M. (2014). Modelling impacts of climate change on global food security. *Climatic Change*, *134*(3), 429–440.

DeFries, R., & Eshleman, K. N. (2004). Land-use change and hydrologic processes: a major focus for the future. *Hydrological Processes*, *18*(11), 2183–2186.
Ekici, A., Lee, H., Lawrence, D. M., Swenson, S. C., & Prigent, C. (2019). Ground subsidence effects on simulating dynamic high-latitude surface inundation under permafrost thaw using CLM5. *Geoscientific Model Development*, *12*(12), 5291–5300.
Fisher, R. A., Wieder, W. R., Sanderson, B. M., Koven, C. D., Oleson, K. W., Xu, C., et al. (2019). Parametric controls on vegetation responses to biogeochemical forcing in the CLM5. *Journal of Advances in Modeling Earth Systems*, *11*(9), 2879–2895.
Galloway, J. N., Dentener, F. J., Capone, D. G., Boyer, E. W., Howarth, R. W., Seitzinger, S. P., et al. (2004). Nitrogen cycles: Past, present, and future. *Biogeochemistry*, *70*(2), 153–226.
Gao, Y., Leung, L. R., Lu, J., Liu, Y., Huang, M., & Qian, Y. (2014). Robust spring drying in the southwestern US and seasonal migration of wet/dry patterns in a warmer climate. *Geophysical Research Letters*, *41*(5), 1745–1751. https://doi.org/10.1002/2014GL059562
Gee, G. W., Oostrom, M., Freshley, M. D., Rockhold, M. L., & Zachara, J. M. (2007). Hanford site vadose zone studies: An overview. *Vadose Zone Journal*, *6*(4), 899–905.
Hatfield, J. L., Sauer, T. J., & Prueger, J. H. (2001). Managing soils to achieve greater water use efficiency. *Agronomy Journal*, *93*(2), 271–280.
Hejazi, M. I., Voisin, N., Liu, L., Bramer, L. M., Fortin, D. C., Hathaway, J. E., et al. (2015). 21st century United States emissions mitigation could increase water stress more than the climate change it is mitigating. *Proceedings of the National Academy of Sciences of the United States of America*, *112*(34), 10635–10640.
Hoegh-Guldberg, O., Jacob, D., Taylor, M., Bindi, M., Brown, S., Camilloni, I., et al. (2018). Impacts of 1.5ºC global warming on natural and human systems. In Masson-Delmotte, V., Zhai, P., Pörtner, H. O., Roberts, D., Skea, J., Shukla, P. R., et al. (Eds.), *Global Warming of 1.5° C: An IPCC Special Report on the impacts of global warming of 1.5° C above pre-industrial levels and related global greenhouse gas emission pathways, in the context of strengthening the global response to the threat of climate change, sustainable development, and efforts to eradicate poverty*: IPCC. Retrieved from https://www.ipcc.ch/site/assets/uploads/sites/2/2019/06/SR15_Chapter3_Low_Res.pdf
Huang, J., Guan, X., & Ji, F. (2012). Enhanced cold-season warming in semi-arid regions. *Atmospheric Chemistry and Physics*, *12*(12), 5391–5398.
Huang, J., Ji, M., Xie, Y., Wang, S., He, Y., & Ran, J. (2015). Global semi-arid climate change over last 60 years. *Climate Dynamics*, *46*(3–4), 1131–1150.
Huang, J., Yu, H., Guan, X., Wang, G., & Guo, R. (2015). Accelerated dryland expansion under climate change. *Nature Climate Change*, *6*(2), 166–171.
Hungate, B. A., Reichstein, M., Dijkstra, P., Johnson, D., Hymus, G., Tenhunen, J., et al. (2002). Evapotranspiration and soil water content in a scrub-oak woodland under carbon dioxide enrichment. *Global Change Biology*, *8*(3), 289–298.
Huntzinger, D. N., Schwalm, C., Michalak, A., Schaefer, K., King, A., Wei, Y., et al. (2013). The North American carbon program multi-scale synthesis and terrestrial model intercomparison project–part 1: Overview and experimental design. *Geoscientific Model Development Discussions*, *6*, 2121–2133.
Hurtt, G. C., Chini, L., Sahajpal, R., Frolking, S., Bodirsky, B. L., Calvin, K., et al. (2020). Harmonization of global land use change and management for the period 850–2100 (LUH2) for CMIP6. *Geoscientific Model Development*, *13*(11), 5425–5464.
Kennedy, D., Swenson, S., Oleson, K. W., Lawrence, D. M., Fisher, R., Lola da Costa, A. C., & Gentine, P. (2019). Implementing plant hydraulics in the Community Land Model, version 5. *Journal of Advances in Modeling Earth Systems*, *11*(2), 485–513.
Kraucunas, I., Clarke, L., Dirks, J., Hathaway, J., Hejazi, M., Hibbard, K., et al. (2015). Investigating the nexus of climate, energy, water, and land at decision-relevant scales: The Platform for Regional Integrated Modeling and Analysis (PRIMA). *Climatic Change*, *129*(3–4), 573–588.
Lawrence, D. M., Fisher, R. A., Koven, C. D., Oleson, K. W., Swenson, S. C., Bonan, G., et al. (2019). The Community Land Model version 5: Description of new features, benchmarking, and impact of forcing uncertainty. *Journal of Advances in Modeling Earth Systems*, *11*, 4245–4287. https://doi.org/10.1029/2018MS001583
Le Quéré, C., Raupach, M. R., Canadell, J. G., Marland, G., Bopp, L., Ciais, P., et al. (2009). Trends in the sources and sinks of carbon dioxide. *Nature Geoscience*, *2*(12), 831–836.
Leakey, A. D., Ainsworth, E. A., Bernacchi, C. J., Rogers, A., Long, S. P., & Ort, D. R. (2009). Elevated CO_2 effects on plant carbon, nitrogen, and water relations: six important lessons from FACE. *Journal of Experimental Botany*, *60*(10), 2859–2876.
Lee, M., Manning, P., Rist, J., Power, S. A., & Marsh, C. (2010). A global comparison of grassland biomass responses to CO_2 and nitrogen enrichment. *Philosophical Transactions of the Royal Society of London B Biological Sciences*, *365*(1549), 2047–2056.
Levis, S., Foley, J. A., & Pollard, D. (2000). Large-scale vegetation feedbacks on a doubled CO_2 climate. *Journal of Climate*, *13*(7), 1313–1325.
Li, Z., Liu, W.-Z., Zhang, X.-C., & Zheng, F.-L. (2011). Assessing the site-specific impacts of climate change on hydrology, soil erosion and crop yields in the Loess Plateau of China. *Climatic Change*, *105*(1–2), 223–242.
Liu, S., Zhuang, Q., He, Y., Noormets, A., Chen, J., & Gu, L. (2016). Evaluating atmospheric CO_2 effects on gross primary productivity and net ecosystem exchanges of terrestrial ecosystems in the conterminous United States using the AmeriFlux data and an artificial neural network approach. *Agricultural and Forest Meteorology*, *220*, 38–49.
Lombardozzi, D. L., Lu, Y., Lawrence, P. J., Lawrence, D. M., Swenson, S., Oleson, K. W., et al. (2020). Simulating agriculture in the Community Land Model version 5. *Journal of Geophysical Research: Biogeosciences*, *125*(8), e2019JG005529. https://doi.org/10.1029/2019JG005529
Lovelli, S., Perniola, M., Di Tommaso, T., Ventrella, D., Moriondo, M., & Amato, M. (2010). Effects of rising atmospheric CO_2 on crop evapotranspiration in a Mediterranean area. *Agricultural Water Management*, *97*(9), 1287–1292.
Lu, Y., Williams, I. N., Bagley, J. E., Torn, M. S., & Kueppers, L. M. (2017). Representing winter wheat in the Community Land Model (version 4.5). *Geoscientific Model Development*, *10*(5), 1873–1888.
Magnani, F., Mencuccini, M., Borghetti, M., Berbigier, P., Berninger, F., Delzon, S., et al. (2007). The human footprint in the carbon cycle of temperate and boreal forests. *Nature*, *447*(7146), 848–850.
McCarthy, H. R., Oren, R., Johnsen, K. H., Gallet-Budynek, A., Pritchard, S. G., Cook, C. W., et al. (2010). Re-assessment of plant carbon dynamics at the Duke free-air CO(2) enrichment site: interactions of atmospheric [CO(2)] with nitrogen and water availability over stand development. *New Phytologist*, *185*(2), 514–528.
McGuire, A. D., Melillo, J. M., & Joyce, L. A. (1995). The role of nitrogen in the response of forest net primary production to elevated atmospheric carbon dioxide. *Annual Review of Ecology and Systematics*, *26*(1), 473–503.
McKenney, M. S., & Rosenberg, N. J. (1993). Sensitivity of some potential evapotranspiration estimation methods to climate change. *Agricultural and Forest Meteorology*, *64*(1–2), 81–110.
Melillo, J. M., Richmond, T., & Yohe, G. W. (2014). *Climate change impacts in the United States: The third national climate assessment*. Retrieved from https://nca2014.globalchange.gov/.

Miles, E. L., Snover, A. K., Hamlet, A. F., Callahan, B., & Fluharty, D. (2000). Pacific Northwest regional assessment: The impacts of climate variability and climate change on the water resources of the columbia River basin 1. *JAWRA Journal of the American Water Resources Association*, *36*(2), 399–420.

Mote, P. W., Parson, E. A., Hamlet, A. F., Keeton, W. S., Lettenmaier, D., Mantua, N., et al. (2003). Preparing for climatic change: The water, salmon, and forests of the Pacific Northwest. *Climatic Change*, *61*(1–2), 45–88.

Niu, J., Sivakumar, B., & Chen, J. (2013). Impacts of increased CO_2 on the hydrologic response over the Xijiang (West River) basin, South China. *Journal of Hydrology*, *505*, 218–227.

Pritchard, S. G., Rogers, H. H., Prior, S. A., & Peterson, C. M. (1999). Elevated CO_2 and plant structure: a review. *Global Change Biology*, *5*(7), 807–837.

Pu, B., & Dickinson, R. E. (2014). Hydrological changes in the climate system from leaf responses to increasing CO_2. *Climate Dynamics*, *42*(7–8), 1905–1923.

Rind, D., Rosenzweig, C., & Goldberg, R. (1992). Modelling the hydrological cycle in assessments of climate change. *Nature*, *358*(6382), 119–122.

Saxe, H., Ellsworth, D. S., & Heath, J. (1998). Tree and forest functioning in an enriched CO_2 atmosphere. *New Phytologist*, *139*(3), 395–436.

Schilling, K. E., Jha, M. K., Zhang, Y. K., Gassman, P. W., & Wolter, C. F. (2008). Impact of land use and land cover change on the water balance of a large agricultural watershed: Historical effects and future directions. *Water Resources Research*, *44*(7), W00A09. https://doi.org/10.1029/2007WR006644

Schimel, D., Stephens, B. B., & Fisher, J. B. (2015). Effect of increasing CO_2 on the terrestrial carbon cycle. *Proceedings of the National Academy of Sciences of the United States of America*, *112*(2), 436–441.

Shi, M., Fisher, J. B., Brzostek, E. R., & Phillips, R. P. (2016). Carbon cost of plant nitrogen acquisition: Global carbon cycle impact from an improved plant nitrogen cycle in the Community Land Model. *Global Change Biology*, *22*(3), 1299–1314.

Singh, A., Kumar, S., Akula, S., Lawrence, D. M., & Lombardozzi, D. L. (2020). Plant growth nullifies the effect of increased water-use efficiency on streamflow under elevated CO_2 in the southeastern United States. *Geophysical Research Letters*, *47*(4). https://doi.org/10.1029/2019GL086940

Swann, A. L., Hoffman, F. M., Koven, C. D., & Randerson, J. T. (2016). Plant responses to increasing CO_2 reduce estimates of climate impacts on drought severity. *Proceedings of the National Academy of Sciences of the United States of America*, *113*(36), 10019–10024.

Taub, D. (2010). Effects of rising atmospheric concentrations of carbon dioxide on plants. *Nature Education Knowledge*, *1*. Retrieved from https://www.nature.com/scitable/knowledge/library/effects-of-rising-atmospheric-concentrations-of-carbon-13254108/.

USDA Natural Resources Conservation Service. (2020). *US general soil map (STATSGO2)*. Retrieved from https://data.nal.usda.gov/dataset/us-general-soil-map-statsgo2.

Wang, W., Lee, X., Xiao, W., Liu, S., Schultz, N., Wang, Y., et al. (2018). Global lake evaporation accelerated by changes in surface energy allocation in a warmer climate. *Nature Geoscience*, *11*(6), 410–414.

WATER, W. C. (2019). *WMO greenhouse gas bulletin*. Retrieved from https://public.wmo.int/en/media/press-release/greenhouse-gas-concentrations-atmosphere-reach-yet-another-high

Weiss, A., Hays, C. J., & Won, J. (2003). Assessing winter wheat responses to climate change scenarios: A simulation study in the US Great Plains. *Climatic Change*, *58*(1–2), 119–147.

Wood, A. W., Leung, L. R., Sridhar, V., & Lettenmaier, D. (2004). Hydrologic implications of dynamical and statistical approaches to down-scaling climate model outputs. *Climatic Change*, *62*(1–3), 189–216.

Xu, Z., Jiang, Y., Jia, B., & Zhou, G. (2016). Elevated-CO_2 response of stomata and its dependence on environmental factors. *Frontiers of Plant Science*, *7*, 657.

Zhou, T., Voisin, N., Leng, G., Huang, M., & Kraucunas, I. (2018). Sensitivity of regulated flow regimes to climate change in the Western United States. *Journal of Hydrometeorology*, *19*(3), 499–515.

Zhu, B., Huang, M., Cheng, Y., Xie, X., Liu, Y., Zhang, X., et al. (2020). Effects of irrigation on water, carbon, and nitrogen budgets in a semiarid watershed in the Pacific northwest: A modeling study. *Journal of Advances in Modeling Earth Systems*, *12*(9). https://doi.org/10.1029/2019MS001953

Zhu, Q., Jiang, H., Peng, C., Liu, J., Wei, X., Fang, X., et al. (2011). Evaluating the effects of future climate change and elevated CO_2 on the water use efficiency in terrestrial ecosystems of China. *Ecological Modelling*, *222*(14), 2414–2429.